

Influence of Water Vapor Activity during Thermal Annealing of
Sputtered IGZO TFT Devices

A Thesis

Presented to the Faculty of the Graduate School
of Cornell University

In Partial Fulfillment of the Requirement for the Degree of
Master of Science

by

Chen-Yang Chung

August 2013

© 2013 Chen-Yang Chung

ABSTRACT

Thermal annealing of sputtered InGaZnO₄ thin films was studied as a function of annealing ambients under controlled partial pressures of oxygen and water vapor.

Water vapor is shown to be critical for obtaining high performance devices with performance improving at water vapor levels substantially higher than normally present in air. The optimized performance of non-reactive sputter fabricated IGZO devices was obtained with post-annealing in air with a 4.5 Torr water vapor pressure.

We propose that, in the post-annealing process, water vapor plays a key role due to its small size and high diffusivity, compared to molecular oxygen, allowing it to more easily compensate oxygen vacancies in the IGZO matrix.

BIOGRAPHICAL SKETCH

Chen-Yang Chung graduated from Chemical Engineering with a minor in Economic from National Taiwan University in 2010. At the National Taiwan University, he completed two projects in Prof. Chung-Hsin Lu's group and published the work as first-author in the Journal of the American Ceramic Society and the Journal of Alloys and Compounds. The first project involved the mechanism of nest-like photoluminescence in $\text{YBO}_3 : \text{Tb}^{3+}$ nanoparticles formed by the microemulsion-mediated hydrothermal method, and the second focused on the synthesis of photocatalyst BiVO_4 via a reverse-microemulsion technique. After serving as a lieutenant in Taiwan Air Force for one year, he came to Cornell University to pursue Master of Science degree in Prof. Michael Thompson's group. At Cornell, his work has focused on IGZO TFT including both device fabrication and materials characterization. He will be continuing his work in Thompson's group as a Ph.D student.

ACKNOWLEDGEMENTS

Firstly, I have to thank my parents who raised me up and give whatever me I needed. It is my pleasure to be their son. They have always supported me whenever I met problems. Secondly, I am very lucky to have made the decision to join Prof. Michael Thompson's team. Our boss, Prof. Thompson, is a genius without any suspicion. He is not only kind to us, but also gave me a lot of useful suggestion in my research. Prof. Dieter Ast has tremendous experiences in semiconductor world and willing to share his extremely useful knowledge with us. It is our pleasure to work with him. Finally, my subgroup teammates Bin Zhu, David Lynch, Ackerley Tng have been a great benefit to me and to each other. Bin has a circumspect mind that prevent us from missing some trivial but important parts in experiments. Although David faced his Q exam, he still worked really hard on our research. We also learn useful electrical engineering from Ackerley who helped us to solve the current leakage problem of Van Der Paaw tool. Adrain Tung, a PhD student in Prof. Edwin Kan's group, also gave me a lot of useful suggestion and was willing to share his experiences. Last but not least, my other labmates Byungki Jung, Alan Jacobs and Bob Bell also gave us some good suggestions and helped us to deal

with critical questions. I also would like to thank Raymond Greene, Corning Inc., Cornell NanoScale Facility (Grant ECCS-0335765), and Cornell Center for Materials Research (Grant DMR-1120296. I am happy to work with the people mentioned above and hope that we will have other amazing breakthroughs in the future together!

TABLE OF CONTENTS

1. Introduction.....	1
2. Literature Review	4
2.1 Advantage of AOS	4
2.2 The feasibility of AOS device fabrication in industry	5
2.3 Advantages of IGZO as a candidate AOS material	6
3 Experimental Details	7
3.1 Thin Film Deposition Techniques- PVD and CVD	7
3.1.1 Sputter Deposition	9
3.1.2 Evaporation Deposition	17
3.1.3 Oxidation	19
3.2 Photolithography	21
3.3 TFT Device Fabrication.....	26
3.4 Post-sputter Annealing	27
3.5 TFT Evaluation	30
4 Results and Discussion.....	34
4.1 Deposition Condition.....	34
4.1 Reactive v.s. Non-reactive Sputtering	36
4.3 Dry Air and Wet Air Post-sputter Annealing Ambients	38
4.4 Role of O₂, N₂ and H₂O in post-sputter annealing.....	43
4.4.1 O₂ post-sputter annealing.....	43
4.4.2 N₂ post-sputter annealing.....	44
4.4.3 O₂ with water vapor post-sputter annealing.....	46
4.4.4 O₂ with water vapor versus wet air post-sputter annealing	47
5 Summary.....	50
6 Conclusions.....	51
7 Future Work.....	52
8 Referencess	53

LIST OF FIGURES

Figures

1. (a) sp ³ hybridized orbitals of a-Si:H and (b) spherical orbitals of AOS.	4
2. Atom/Molecule interaction with substrate during thin film deposition	9
3. DC Diode Sputtering Deposition.	12
4. Crookes Dark Space in Sputter Deposition	13
5. RF Sputter System.	15
6. Magnetron sputter	16
7. Thermal Evaporation deposition.	18
8. E-beam Evaporation deposition	19
9. Mass-transport limited and reaction-rate limited region in CVD deposition	20
10. Scheme of Oxidation	21
11. Scheme of Photolithography process.	23
12. Priming with HMDS before spinning on photoresist.	24
13. Lift off photolithography process	25
14. IGZO bottom gate TFT test structure.	27
15. UHV compatible annealing furnace with gas ambient control. The hot zone is quartz to prevent sample contamination. Annealing ambient is controlled by varying the relative flow rates.	28
16. The relation of saturated water vapor pressure and water bath temperatures..	29
17. I _{DS} -V _{DS} curve	32
18. Fitting line of saturation current versus V _{GS} curve	33
19. I _{DS} -V _{GS} curve at V _{DS} = 10V	34
20. Sputter deposition rate at different powers and pressures	35
21. Schematics of IGZO a) as-deposited, showing high conductivity, and b) post-anneal in oxygen-containing ambient, showing reduced vacancy and carrier concentration.	37
22. I _{DS} -V _{GS} curve of IGZO device post-annealed in dry air and normal air.	39
23. Transfer characteristics of IGZO devices post-annealed in air ambient with	

varying water vapor content. V_{DS} is 10V for all traces.	40
24. Sub-threshold slope of IGZO devices post-annealed in air ambient with varying water vapor content.	41
25. Mobility and on voltage of IGZO devices post-sputter annealed in air ambient with varying water vapor content.	43
26. I_{DS} - V_{GS} curves of IGZO TFTs post-sputter annealing in ambient of pure O_2 and dry air..	44
27. I_{DS} - V_{GS} curves of IGZO TFTs post-sputter annealed in pure N_2 , N_2 with 9 Torr water vapor and dry air	46
28. I_{DS} - V_{GS} curves of IGZO TFTs post-sputter annealed in pure O_2 and O_2 with 9 Torr water vapor..	47
29. Comparison of transfer characteristics of IGZO devices post-annealed in oxygen and dry air with 4.5 Torr water vapor	48

LIST OF TABLES

Tables

1. Comparison of practical AOS compounds based on Zn, Ga, In and Sn.....**6**
2. Post-sputter annealing ambients studies**39**
3. Performance results of all IGZO devices in different conditions**49**

1. Introduction

Amorphous semiconductors, primarily a-Si, have dominated the solar cells and active-matrix (AM) flat-panel display market. Single-crystalline semiconductors, typified by c-Si, are generally unsuitable for such applications because they cannot be uniformly formed over large areas ($>1 \text{ m}^2$) at low temperature (e.g. $< 400 \text{ }^\circ\text{C}$) on glass or plastic substrates. Due to defect trapping and carrier scattering on grain boundaries in polycrystalline materials, amorphous materials such as hydrogenated amorphous silicon (a-Si:H), have been used more widely used for large-size applications. However, the drawbacks of low mobility ($< 1 \text{ cm}^2/\text{V s}$) and the instability under electric stress and photo-illumination still limit a-Si:H based devices in more advanced circuit applications. [1]

In 2004, Hosono reported that an amorphous oxide semiconductor (AOS) with the composition a-InGaZnO_4 (a-IGZO) could be used in the fabrication of transparent and flexible thin film transistors (TFTs) with significantly improved performance compared to conventional a-Si:H based TFTs [2]. Since AOS materials have shown tremendous promise as a replacement for amorphous silicon (a-Si), much work has focused on optimizing properties of IGZO by controlling process variables

including channel layer stoichiometry [3], reactive sputtering O₂ partial pressure [4], channel layer thickness[5], and post-sputter annealing [6]. Some level of post-sputter annealing is almost always required to achieve stable high performance devices. Previous work studying the effects of annealing temperature [6][7]and ambient environment [8] [9] [10]show a strong influence of these parameters on device performance. In 2008, Nomura et al [11] studied the role of water vapor (H₂O) in an oxygen (O₂) annealing ambient on device performance, finding that the average saturation mobility increased from 9.3 cm²/V-s in dry oxygen to 11.8 cm²/V-s in ambients with nearly 50% water vapor. Shin et al. [10] similarly studied annealing in “wet” nitrogen at water partial pressures to 0.5 atm and total pressures as high as 5 atm. Device mobility was found to improve from 7.7 to 13.2 cm²/V-s with increasing H₂O partial pressure. However, no systematic study of this behavior has been reported to date.

In this work, we focus on the optimization of IGZO device performance by control of all of the gas components in the post-sputter annealing environment, including p_{N₂}, p_{O₂}, and p_{H₂O}. Our results show that control of the H₂O partial pressure is critical for achieving high mobility devices. The impact of modifying the

ambient during the thermal annealing has also been explored.

2. Literature Review

2.1 Advantage of AOS

The low mobility of a-Si:H is attributed to the directional nature of the tetrahedral Si sp^3 orbital shown in Fig. 1 (a), which restricts the transport of the electrons in the matrix. In contrast, the dominant spherical orbitals of amorphous oxidize semiconductor (AOS) are shown in Fig. 1 (b). In AOS, the conduction bands is primarily spherical s-type in nature and hence the transport of electrons through the matrix is not as restricted as that of directional orbitals. Moreover, AOS are insensitive to bond angle variance of metal-oxide-metal chemical bonds due to structural randomness inherent in amorphous materials.

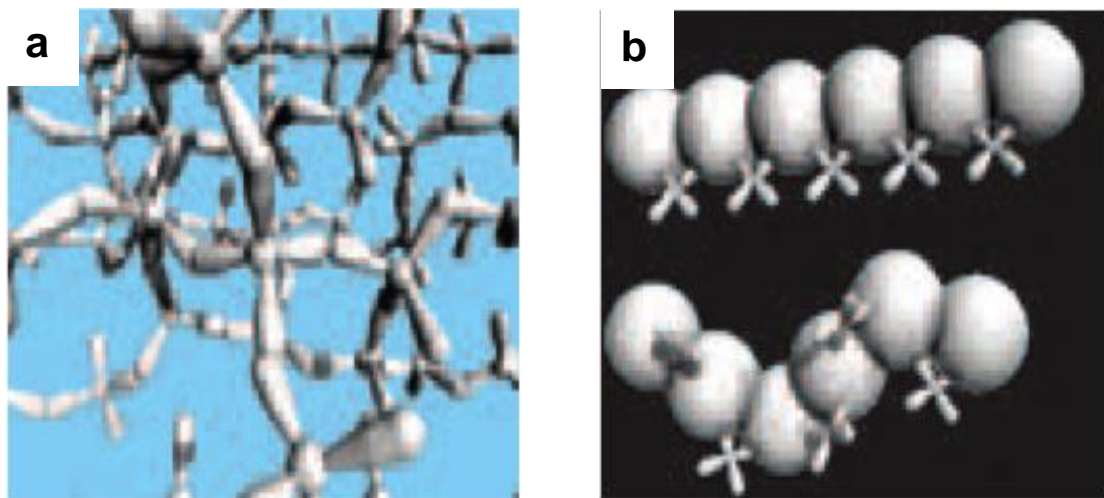


Figure. 1 (a) sp^3 hybridized orbitals of a-Si:H and (b) spherical orbitals of AOS.

Because of the amorphous characteristic, AOS also possess the advantage of low processing temperature and no grain boundaries. The absence of grain boundaries eliminates trapping of electrons at specific structures and generates a more uniform set of properties for large area flat panel displays [1].

2.2 The feasibility of AOS device fabrication in industry

Hosono proposed several candidates elements for AOS materials, including Zn, Cd, Hg, Ga, In, Ti, Ge, Sn and Pb. After excluding the toxic and rare elements among the candidate elements, Zn, In, Ga and Sn have the potential to be used in industry. Table 1 shows several viable compounds based on these four cations. Most of these are removed as candidates because of certain disadvantages in properties or costs. Tin-containing compounds, Zinc-Tin-Oxide (ZTO) and Tin-Gallium-Zinc-Oxide (TGZO) are difficult to etch during fabrication. Although the mobility of Indium-Gallium-Oxide (IGO) and (Indium-Gallium-Zinc-Oxide) IGZO are similar, IGO is much more expensive than IGZO because of higher fraction of expensive In. In Indium-Zinc-Oxide (IZO) and Zinc Oxide (ZnO), the In-O and Zn-O bonds are too weak to prevent oxygen from escaping from the matrix, resulting

in the generation of excess oxygen vacancies. This makes it difficult to turn the transistor off because of the electron doping arising from the excess oxygen vacancies.

Table 1 Comparison of practice AOS compounds based on Zn, Ga, In and Sn

Compound	Etch	Mobility	Transistor turn-off	Price
ZTO	Difficult	–	–	Low
TGZO	Difficult	–	–	Low
IGO	Easy	Good	Easy	High
IZO	Easy	Very good	Difficult	Moderate
ZnO	Easy	Good	Difficult	Low
IGZO	Easy	Good	Easy	Moderate

2.3 Advantages of IGZO as a candidate AOS material

The incorporation of Ga in IZO actually helps to suppress oxygen vacancies since the Ga-O bond is stronger than Zn-O and In-O bonds. By bonding more strongly with oxygen, the undesired electron doping is avoided. A comparative study between a-IZO and a-IGZO has shown that IGZO can have five orders of magnitude lower in carrier concentrations than a-IZO in the off state. Moreover, the crystallization temperature of the multi-component IGZO is higher than the binary-components ZnO because of the more complex structure. This allows higher

processing temperature while retaining the amorphous characteristic. Theoretically, the mobility should be in the range of 10~50 cm²/Vs, dominated by Indium in the amorphous ZnO matrix. In IGZO, the valence band is formed primarily by O 2p and Zn 3d-orbitals, while the conduction band is formed by the s and p orbitals of the three metals with some influence by the O 2p-orbitals. The mobility of IGZO is primarily determined by the fraction of In₂O₃ in agreement with the Hosono working theory since In³⁺ has the largest ionic radius among the metal cations. Finally, IGZO has a wide bandgap (~3eV) and is highly transparent in visible light (with transmittance over 90%). This property opens up to new application including transparent electronics and “see-through” displays. Currently, IGZO is the only material which has been demonstrated to satisfy a balance between high mobility and large area uniformity [12].

3. Experimental Details

3.1 Thin Film Deposition Techniques- PVD and CVD

There are two main methods to deposit thin films on substrates, Physical Vapor Deposition (PVD) and Chemical Vapor Deposition (CVD). In PVD, the target material is excited by a high energy source such as laser beam or electron beam, vaporizing the material and transporting it to the substrate where it condenses. CVD, on the other hand, uses sources supplied in the forms of gases or liquid precursors and deposition occurs following a chemical reaction near or at the substrate. The thin film properties in both cases are highly dependent on uniformity and deposition rate. In many PVD processes, atoms travel in a straight path in high vacuum with few collisions. In contrast, CVD processes are normally carried out at moderate pressure with many collisions of relative species in the gas phase. Thus, in PVD the thin film uniformity is dependent on the supply rate and the geometry of the substrate surface, whereas in a CVD process the thin film uniformity is dependent on the gas or liquid flow patterns and on the source molecule diffusion through the surrounding gases. For PVD process carried out in ultra-high vacuum, there is an additional advantage that access to the deposition surface allows use of analytical techniques involving

electron beams [13]. Many PVD processes can be used to deposit both elemental and alloys films, as well as many compounds via reactive deposition processes. In these reactive deposition processes, an ambient gas environment such as oxygen or nitrogen is employed to form oxides and nitrides [14]. Many PVD processes are generally divided into three major categories, sputtering, evaporation and ablation. We discuss primarily sputtering as this is used to deposit IGZO. Low Pressure CVD (LPCVD), which is also used in this research, is also introduced.

3.1.1 Sputter Deposition

IGZO is most commonly deposited by sputtering from either ceramic targets or by reactive sputtering from multiple metal targets. Film deposition during sputtering can be described in terms of several sub-steps as shown in Figure 2.

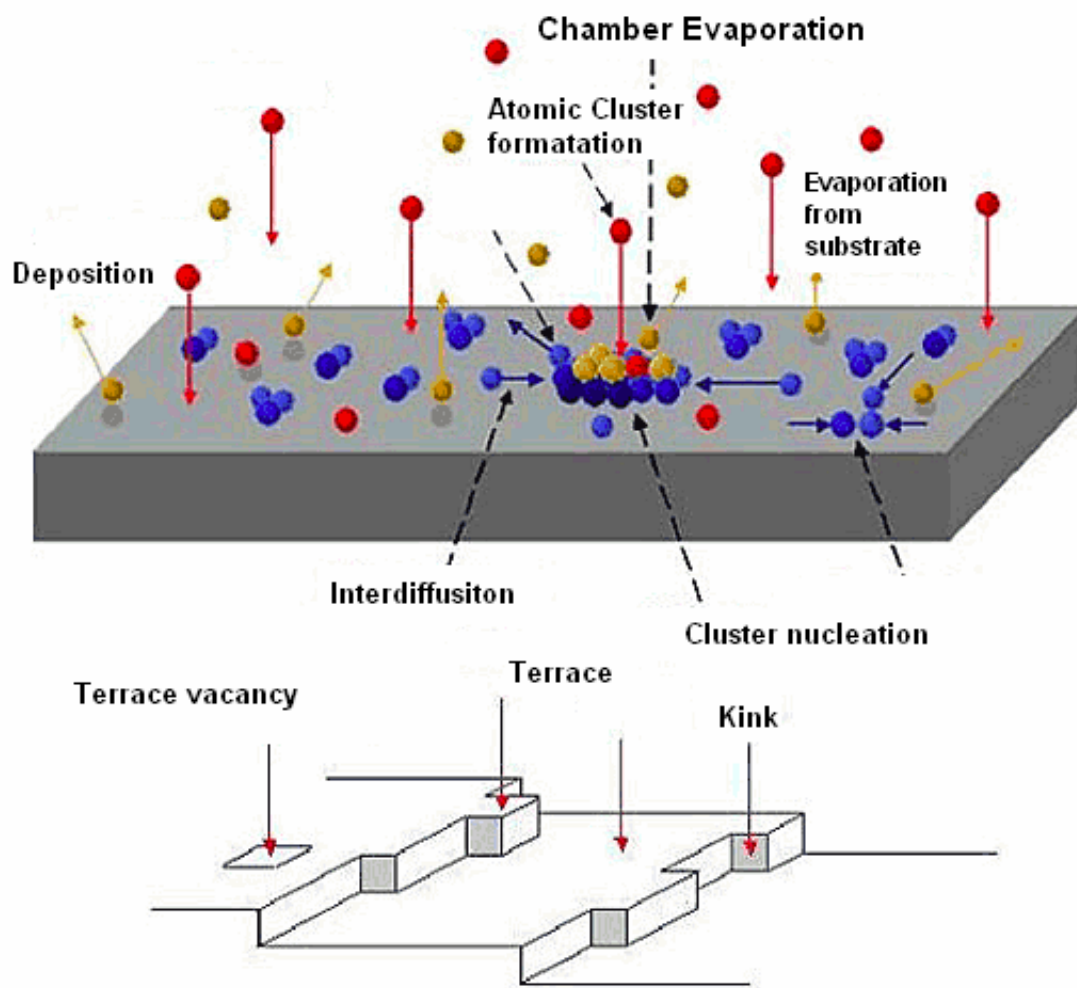


Figure 2. Atom/Molecule interaction with substrate during thin film deposition

During sputtering, atoms and molecules arrive at the surface with moderate energy and are absorbed onto the substrate. To reach lower energy states bonds must be broken between the absorbed molecules and the surface so that the molecules can move to new locations and form new bonds. In the surface diffusion step, the atoms or molecules interact within themselves and form larger clusters. Below a critical cluster size (nucleation), these clusters are thermodynamically unstable and may

desorb depending on the deposition parameters. After reaching a certain size, the clusters become thermodynamically stable and an equilibrium density of clusters exist on the substrate. The critical nuclei grow in number and in size until the saturation nucleation density is reached. The nucleation density and the size depends on parameters including the rate of impingement, the activation energy for adsorption, desorption, energy of the impingement, thermal diffusion, temperature, topography, and chemical properties of the substrate. A nucleus can grow both parallel to the substrate by surface diffusion of the adsorbed species, and perpendicular to substrate surface by direct impingement of the incident species. Generally, the rate of parallel growth on the substrate is much higher than that of perpendicular growth. In the coalescence step, small island nuclei coalesce with each other to reduce the islands' surface energy. This tendency to form larger islands, agglomeration, can be enhanced by increasing the surface mobility of the adsorbed species, such as by increasing the substrate temperature. Larger islands grow together, leaving holes and channels of uncovered substrate. These holes and channels are filled until a completely continuous film forms.

In the growing film, there are kink and terrace sites shown in Figure 2.

Adsorbed species tend to be more stable on kink sites compare to terrace or other island sites because of the additional bonding. Under these conditions, the growth is termed step growth. [15]

When a solid surface is bombarded with energetic particles such as accelerated ions, surface atoms of the solid are scattered backward due to collisions between the surface atoms and the energetic particles. This phenomenon is termed sputtering. Several sputtering systems can be employed for thin film deposition including dc diode, rf diode, magnetron, and ion beam sputtering. A dc sputtering system is composed of a pair of planar electrodes, (cathode and anode) as shown in Figure 3.

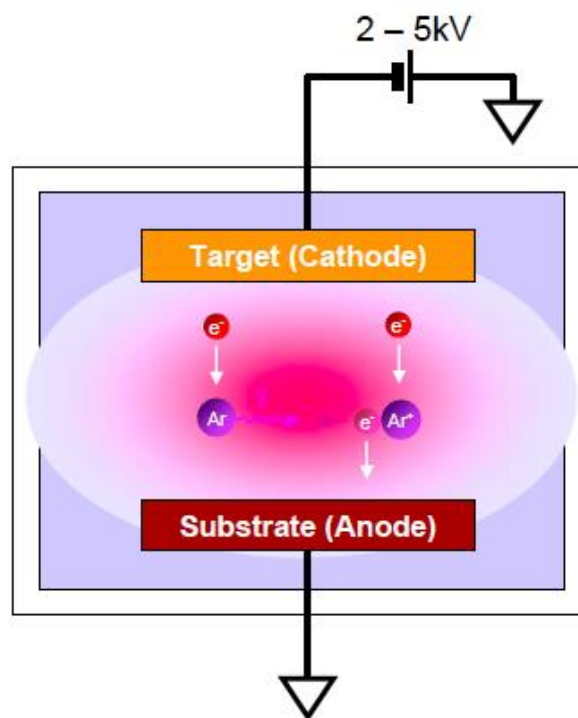


Figure 3. DC Diode Sputtering Deposition

The surface of the cathode is covered with the desired deposition material, while the substrates are placed on the anode. The sputtering chamber is filled with sputtering gas, usually Ar since it is relatively heavy and unreactive. An applied electric field accelerates the initially small number of free electrons in the chamber, which then inelastically collide with neutral Ar atoms. The inelastic collision excites the Ar atom to a positive ion. These Ar ions are then accelerated by the electric field and bombard the cathode target surface with momentum transfer, contributing to backward dislodgement of target material molecules and electrons. The sputtered electrons, called secondary electrons, strike other neutral Ar atoms in chamber to form additional positive Ar ions to sustain the process. The sputtered target atoms both drift and are accelerated to the anode where they result in the deposition of thin film on the substrate and chamber wall. The common pink glow discharge of the plasma results from the excitation of Ar.

Near the cathode, electrons move faster than Ar ions due to their smaller mass. Thus positive charges build up near cathode, raising the potential of the plasma and fewer electrons collide with neutral Ar. Thus, as shown in Figure 4, there are fewer

excited Ar ions near the cathode leading to dark space sheath, called Crookes dark space.

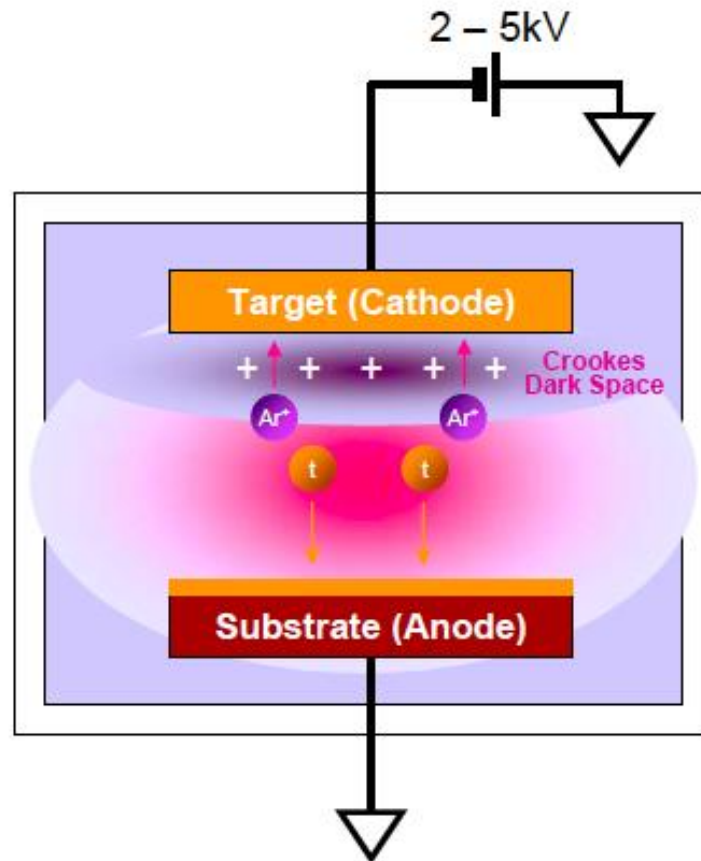


Figure 4 Crookes Dark Space in Sputter Deposition

If the target is not conductive (i.e. an insulator or semiconductor), positive charge would also accumulate on cathode target surface during Ar ion bombardment. This would reduce the potential difference between the plasma and the cathode. In order to sustain the glow discharge with insulator targets, high frequency (rf) voltage is applied to the target instead of DC. The insulator target is alternately ion and

electron bombarded. Positive charges which accumulate on target surface during the negative cycle are neutralized by electrons during the positive cycle. Thus in RF plasma, there are two dark space sheath, which are ion accelerating zones, one near the target and the other one near the substrate as shown in Figure 5.

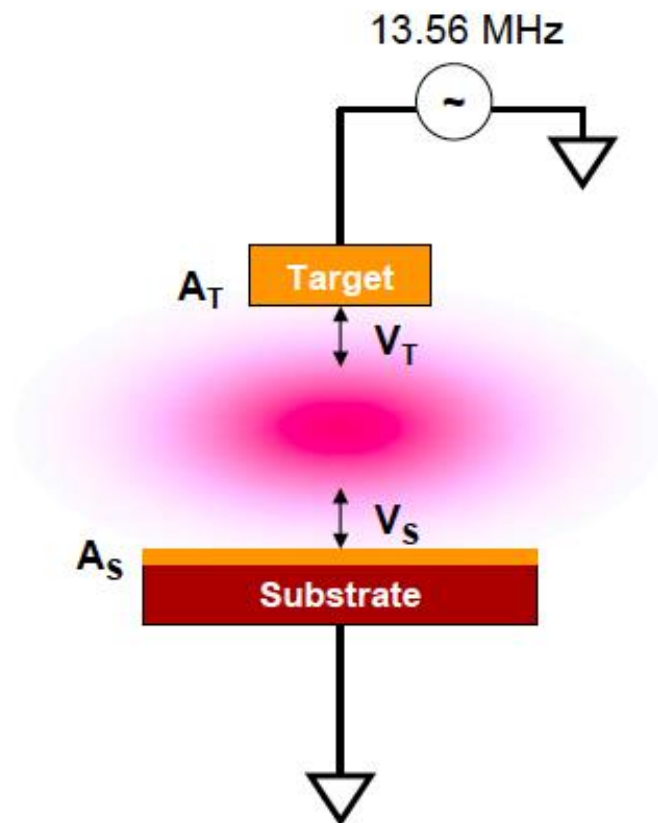


Figure 5 RF sputter system

During an RF discharge, Ar ions not only bombard the target but also the substrate.

The relationship between the substrate, the target potential, and area in an RF sputter system is shown in Eqn. 1,

$$V_T/V_S = (A_S/A_T)^n \quad (1)$$

where V_T is the voltage across the target sheath, V_S is the voltage across the substrate sheath, n usually is 4, A_S is the area of the substrate electrode and A_T is the area of the target electrode. Thus, in order to reduce bombardment of the substrate film, the target area is normally reduced in an RF sputter system. Moreover, the RF frequency has to be high enough that the polarity can alternate before Ar ions pass through the dark space sheath to bombard the anode substrate. Typically, the frequency is 13.56 MHz which is sufficient for electrons to strike on neutral Ar to induce plasma without secondary electrons needed in the beginning [16].

In order to increase the sputter deposition rate, magnetron sputtering is further used in thin film deposition. In magnetron sputter, a parallel magnetic field is applied on the glow discharge as shown in Fig. 6.

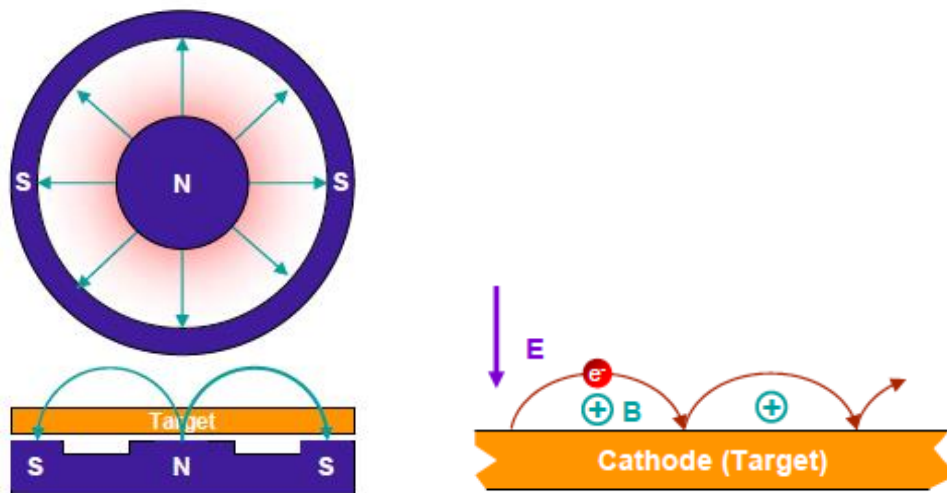


Figure 6 Magnetron sputter

Electrons in the glow discharge undergo cycloid motion, and the drifting orbit is in the direction of the $E \times M$, where E and M denote the electric field in the discharge and the magnetic field. The magnetic field is oriented such that these drift paths for electrons form a closed loop and confine electrons to remain near the target to sustain the plasma. This causes an increased opportunity of collision between the electrons and the sputtering gas molecules. The magnetic field causes the plasma density to increase, leading to increased current density at the cathode and contributes to an increased sputtering rate [17].

3.1.2 Evaporation Deposition

Evaporation is a second PVD method as shown in Figure 7. The source material, loaded in crucible is heated until it thermally evaporates and the vapor is transported to the surface of the substrate. The vapor immediately condenses on the surface of the substrate in a high-vacuum environment.

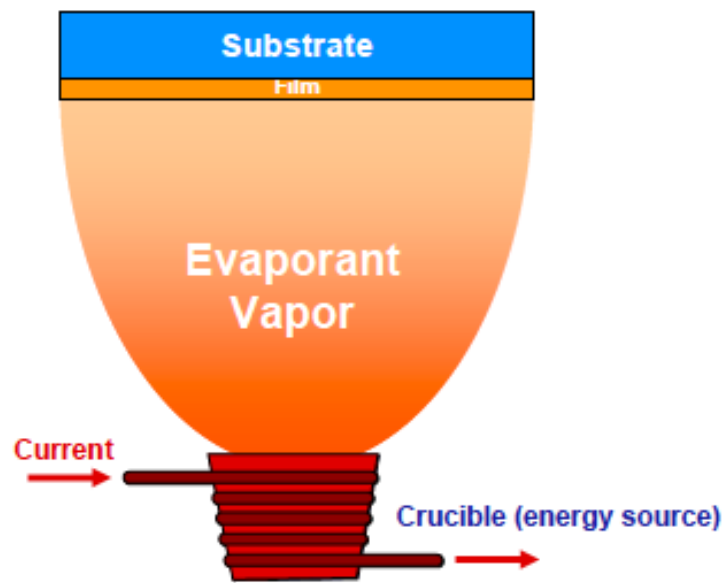


Figure 7. Thermal Evaporation deposition

The melting points of some materials, such as W, Mo and Pt, are so high that they are difficult to thermally evaporate from a crucible. Instead an Electron beam (E-beam) evaporator is required for such high melting point materials. An electron beam (Fig. 8) from a cathode filament is bent by a magnetic field so that it is incident on source material in a crucible. The electron beam heats the material to the vaporization

temperature using the remaining material as a crucible in many cases. Evaporated atoms in both cases travel upward and condense on the substrate [18].

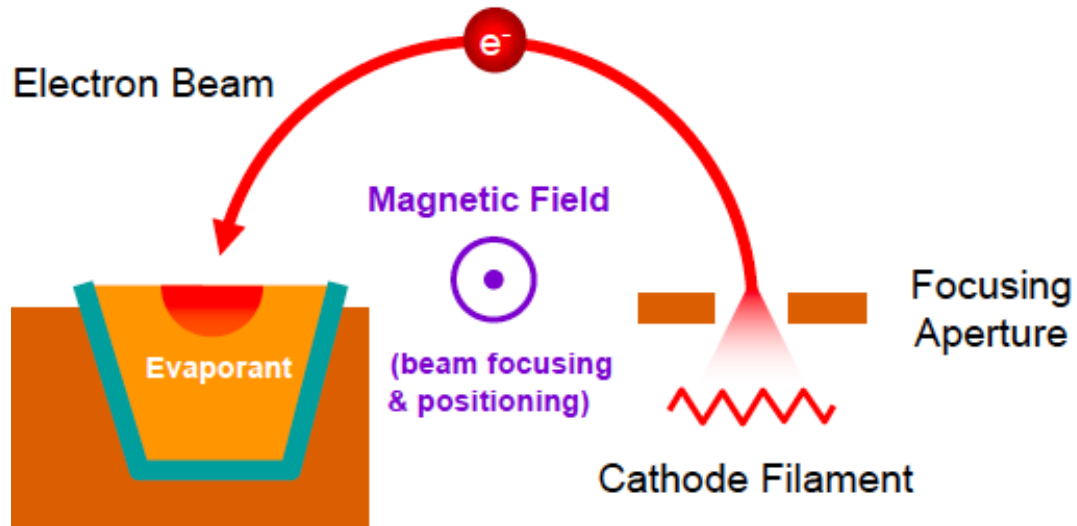


Figure 8. E-beam Evaporation deposition

3.1.3 Oxidation

In CVD or other reactive based deposition techniques, there are both mass-transport limited and reaction-rate limited regimes as shown in Fig. 9. In a mass-transport limited regime, the reaction rate exceeds the arrival rate of reactants, generally due to high processing temperatures. Thus the gas flow characteristics control film deposition and film uniformity depends on whether reactants can be uniformly delivered across a wafer or wafer-to-wafer, while film growth is insensitive to temperature. In the reaction-rate limited regime, the arrival of reactants exceeds

the reaction rate, often the case for low processing temperatures or pressure. The reaction rate controls film deposition and film uniformity depends on temperature uniformity across a wafer or wafer-to-wafer. In most of the cases, engineers prefer the mass-transport limited regime due to the difficulty of controlling chemical reaction temperatures in a fabrication process.

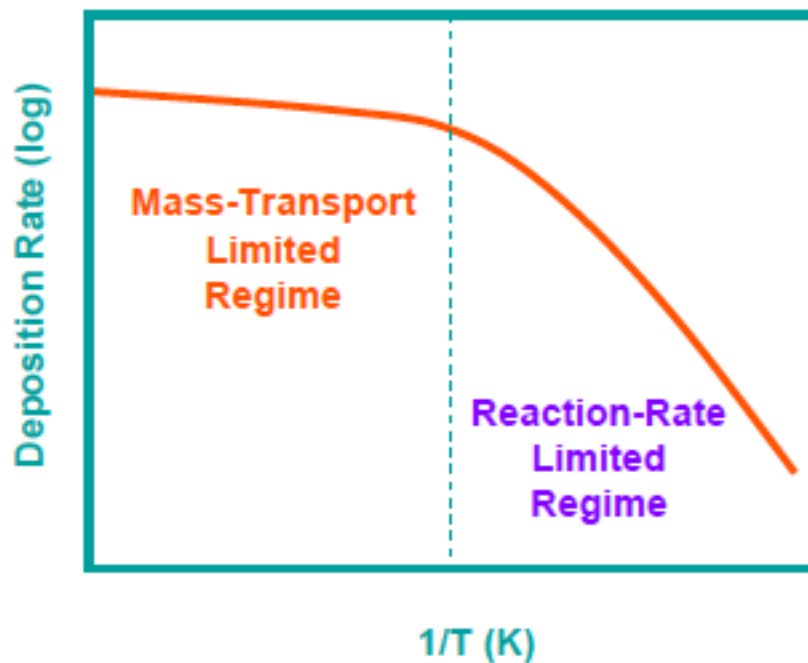


Figure 9. Mass-transport limited and reaction-rate limited region in CVD deposition

Thermal oxidation of silicon is an example of a reaction that can be either mass or reaction rate limited. Oxidation can be done as a dry or wet process. In dry oxidation, Si reacts directly with O_2 to form SiO_2 . Wet oxidation adds water vapor allowing the Si to react also with H_2O to form SiO_2 and H_2 . Dry oxidation occurs

more slowly than wet oxidation, but the quality of the dry oxide is better. Figure 10 shows a typical oxidation furnace with wafers packed close and vertical. In the reaction rate limit, film uniformity can be maintained as long as the temperature is uniform in the chamber. The uniform temperature is controlled by multiple heaters, surrounding the chamber [18].

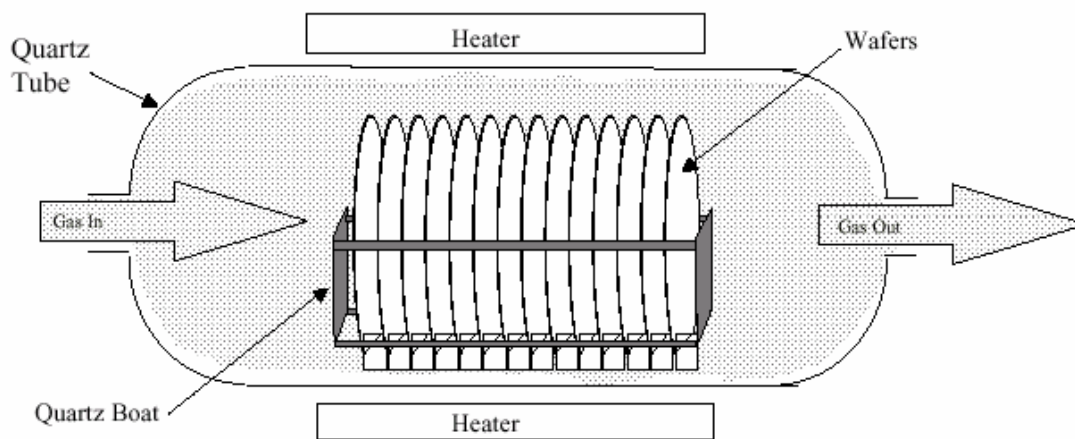


Figure 10. A typical oxidation furnace

3.2 Photolithography

Photolithography is the process using light to transfer a desired geometric pattern from a photomask to a light-sensitive photoresist on the substrate. A series of chemical treatments then transfers the pattern into the underlying material. It is a process mainly employed in microfabrication to pattern thin films. The

photolithography process is demonstrated schematically in Figure 11. Photoresist is first applied by spinning. After spin, a post-apply baking is used to evaporate remaining solvents and to densify the photoresist. The resist is then exposed to UV light (365 nm i-line in this work) through a photomask. The UV exposure modifies the solubility of the resist, making either the exposed (positive resist) or unexposed (negative resist) regions of the resist soluble in a developer. After developing, remaining photoresist acts as a barrier during etching of underlying layers. The residue photoresist is then stripped off and the desired pattern is obtained for subsequent processing.

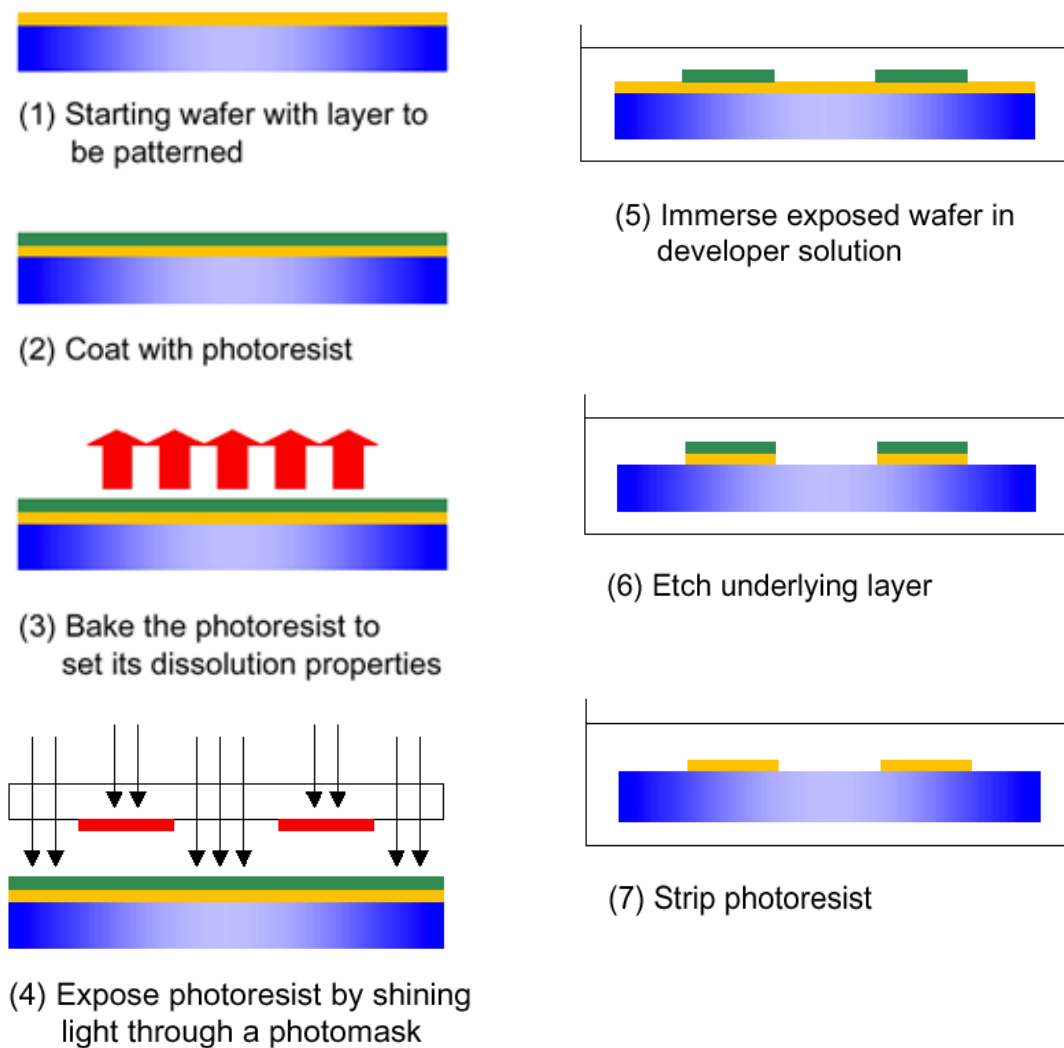


Figure 11. Scheme of Photolithography process

Adhesion of photoresist to an inorganic surface is often a challenge. To improve the performance, the surface is normally primed with HMDS (hexamethyldisilazane) before spinning on photoresist (Figure. 12). The surface of most inorganic materials tends to be hydrophilic when exposed in air. However, the photoresist wants to

adhere to a hydrophobic surface. Thus, the HMDS is spun on the surface before spinning on photoresist to convert the surface from hydrophilic to hydrophobic [19].

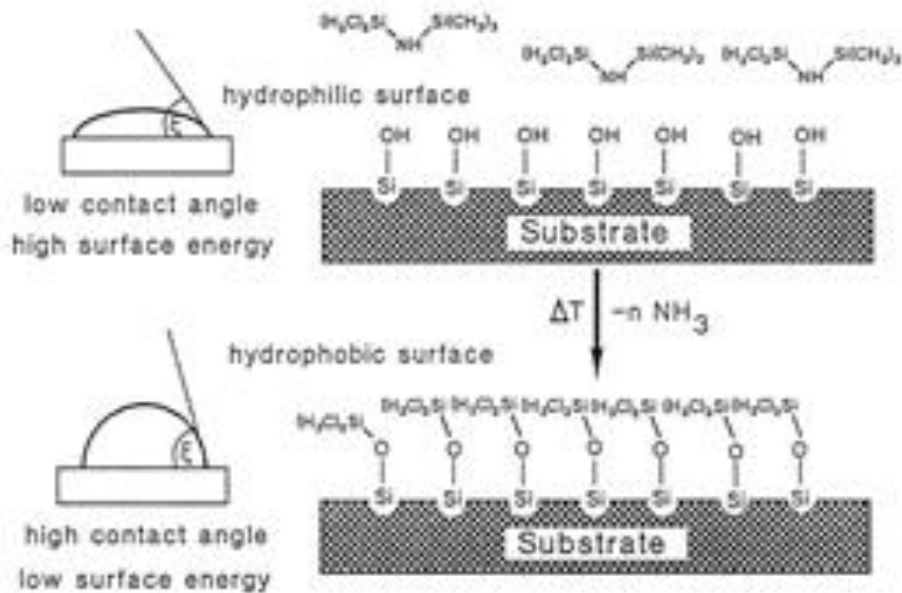


Figure 12. Priming with HMDS before spinning on photoresist [19].

As an alternation to this pattern/etch process, lift off photolithography can be employed as shown in Figure 13 to control addition steps such as evaporation.

Photoresist is spun on the wafer as before followed by UV exposure. The UV exposed areas are then “reversed” in an ammonia bake. The remaining resist is then exposed to UV light and developed normally to leave the chemically modified initial exposure. A thin film may then be deposited by PVD process such as evaporation.

Following the deposition, the resist is removed in a solvent leaving the metal pattern in areas not protected by the resist. The advantage of lift off photolithography is that it does not damage materials underneath the layer, and avoids even exposure to reactive chemicals [19].

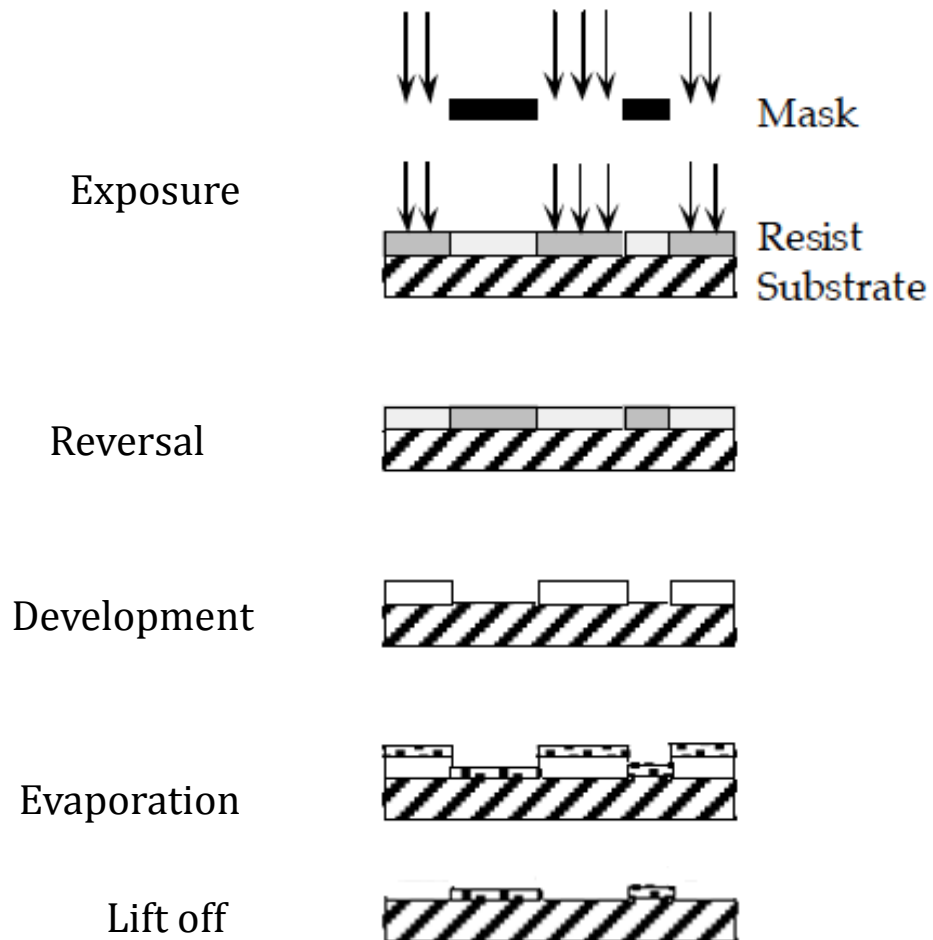


Figure 13 Lift off photolithography process

3.3 TFT device fabrication

The primary method for evaluation of IGZO films was the thin film TFT device. IGZO-based thin film transistors (TFTs) were fabricated using a staggered bottom-gate test structure as shown in Fig. 14 (a). p-doped 4-inch Si substrates (0.01-0.02 Ω -cm) were thermally dry oxidized (1100°C for 30 min with 3% HCl) to grow a 100 nm SiO₂ gate dielectric. The gate via was patterned using 6:1 BOE as shown in Fig. 14 (b). The source and drain electrodes were thermally evaporated and patterned using lift-off photolithography (Fig. 14 (d)). These contact were a stack of Ti (10 nm adhesion), Al (100nm ohmic contact IGZO) and Au (100 nm to reduce contact resistance to probe tips). The channel width (W) and length (L) were 200 and 50 μ m, respectively. IGZO channel layers (Fig. 14 (e)) were deposited via RF magnetron sputtering in a load locked dedicated sputter chamber with a base pressure of 10⁻⁷ Torr under varying conditions. IGZO was deposited from a 2-inch target sintered InGaZnO₄ (1:1:1) target sputtered at a typical pressure of 5 mTorr Ar and at a typical power of 120 W. Following deposition, devices were patterned lithographically and etched in 2 wt.% HCl. As no passivation was added to the structure, devices were tested quickly after fabrication because performance began to

degrade within 1 day (typically 50% loss over 24 hours).

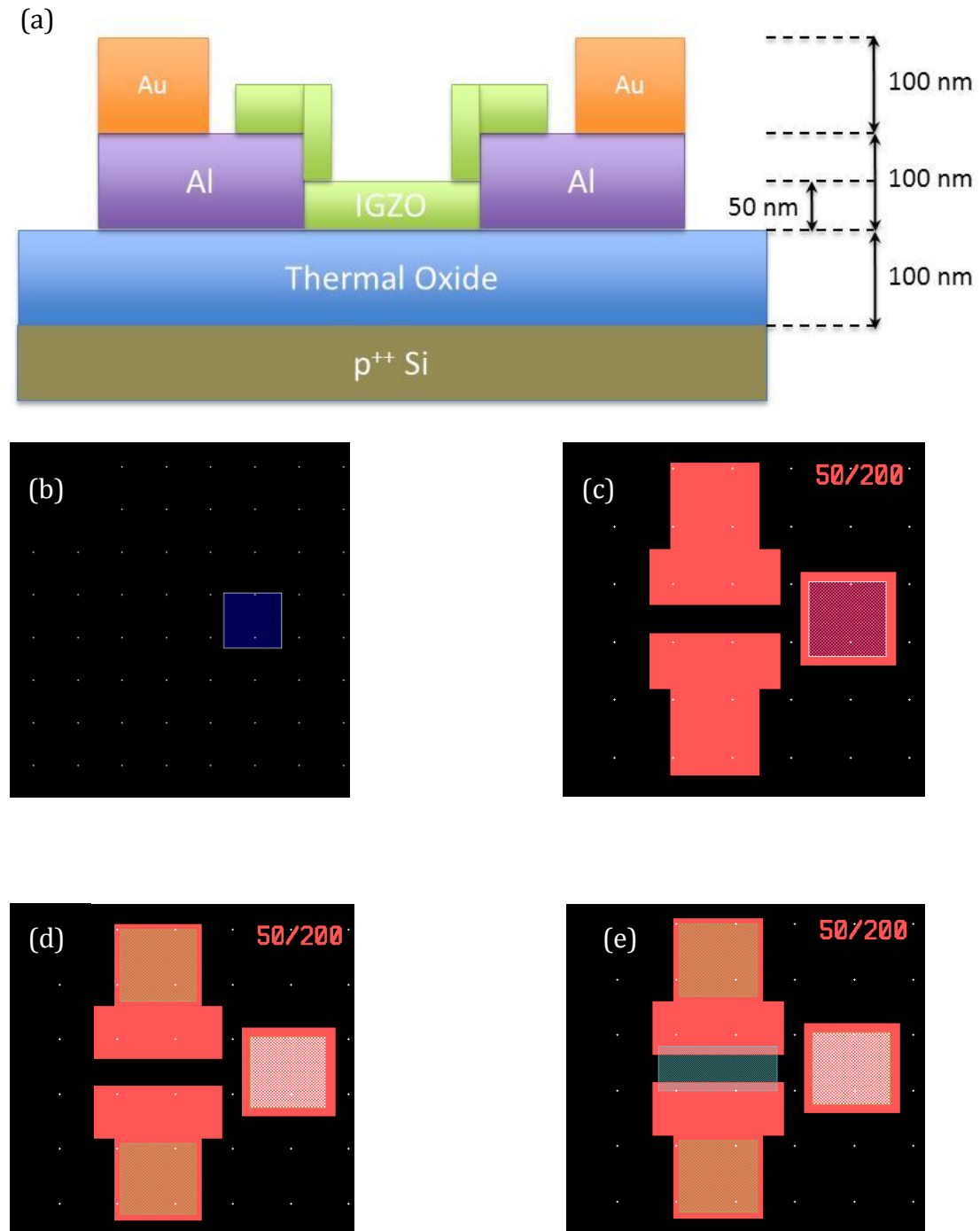


Figure 14 IGZO bottom gate TFT test structure and masks pattern

3.4 Post-sputter annealing

After IGZO deposition and patterning, samples were annealed in a UHV compatible furnace with a dedicated gas delivery system, as shown schematically in Fig. 15. Samples were annealed after patterning to avoid any potential degradation during lithography or the HCl etch.

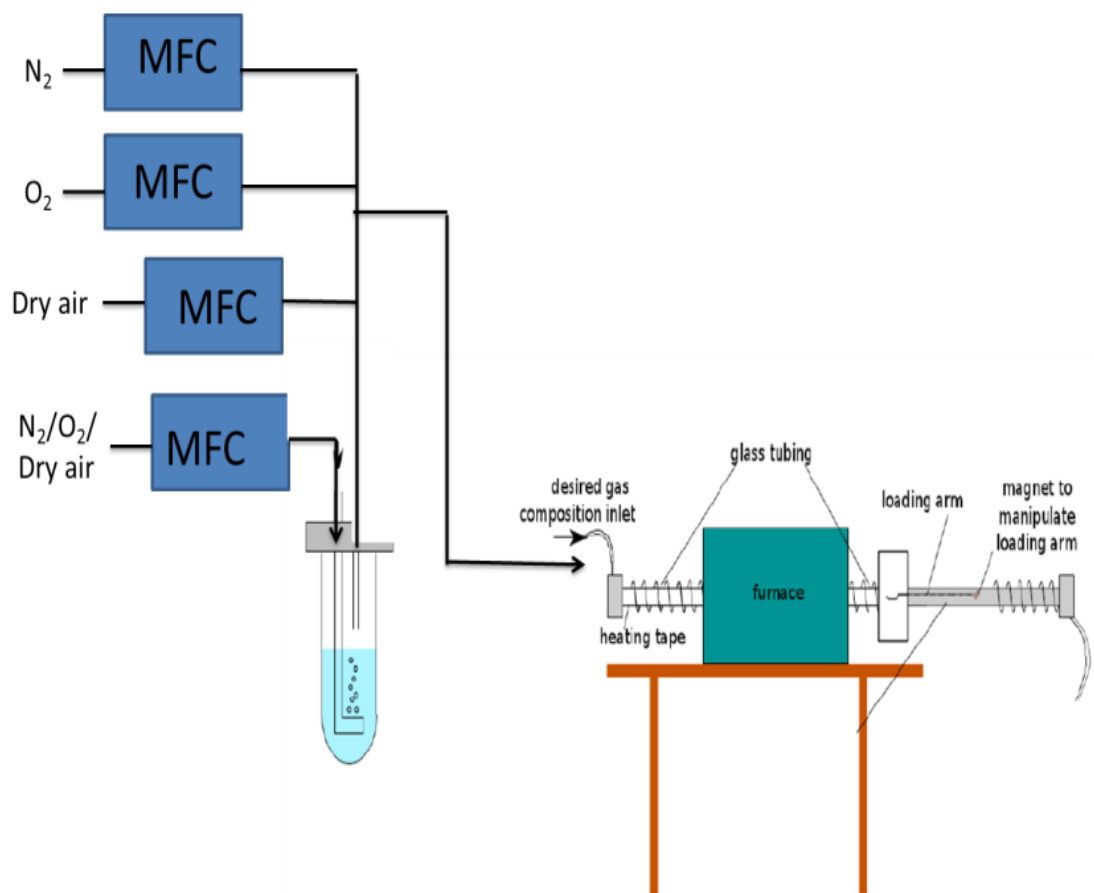


Figure 15. UHV compatible annealing furnace with gas ambient control. The hot zone is quartz to prevent sample contamination. Annealing ambient is controlled by varying the relative flow rate

In contrast to most other studies that use just uncontrolled air for post-sputter

annealing, the atmosphere was carefully controlled during these anneals. Although the furnace is UHV compatible, all anneals were carried out at atmospheric pressure. Flow meters controlled independent lines of nitrogen, oxygen, dry air (-62°C dew point), and water vapor saturated gas allowing arbitrary mixing ratios. Saturated water vapor gases were produced by bubbling nitrogen, oxygen or dry air through a frit immersed in de-ionized (DI) water held at a controlled temperature. A thermal bath for the DI water permitted the dew point of the saturated gas to be varied from 0°C to 30°C . The relation of $P_{\text{H}_2\text{O}}$ in the furnace system with the water bath temperature is shown in Figure 16. The amount of water vapor in furnace system was controlled by varying the temperature setting of the thermal bath.

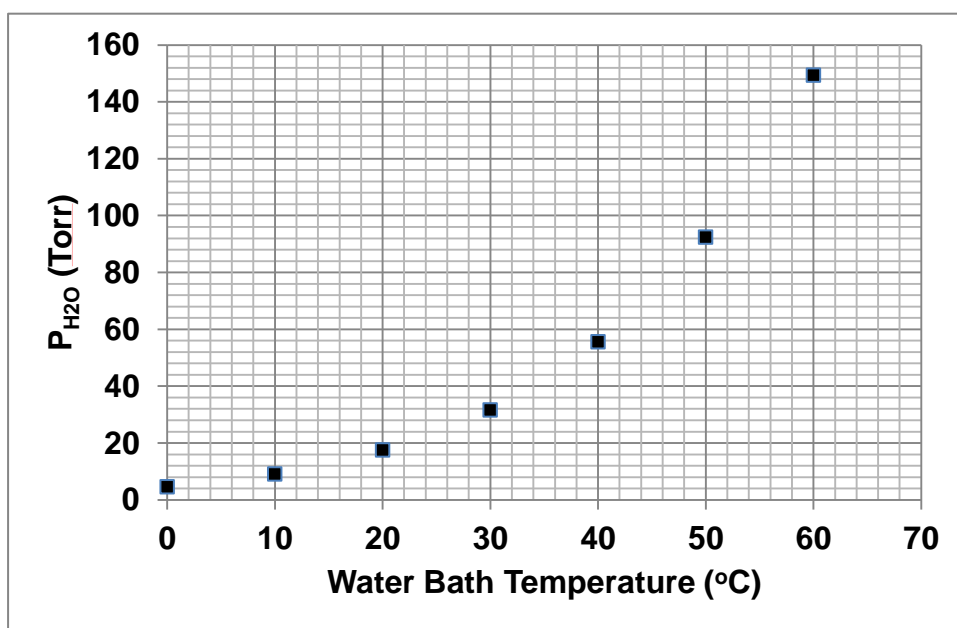


Figure 16. The relation of saturated water vapor pressure and water bath temperatures

To prevent condensation and maintain the $p_{\text{H}_2\text{O}}$, all other components of the furnace were wrapped with heating tape to maintain temperatures above the dew point of the gas mixture. For anneals, samples were loaded into a load-lock at room temperature and the furnace was sealed. Gases flowed for a minimum of 10min before the sample was moved into the furnace zone at flow rate of typically 1100 sccm with a furnace volume of 2550 cm³. The gas exchange time is thus < 2.5 min. Prior to transferring samples to the hot zone of the furnace, the furnace was flushed with the process gas for 10 minutes. During anneals, the ambient gas was normally maintained as the sample cooled. However, experiments were also performed where the ambient was switched to dry N₂ or O₂ just prior to removing the sample from the heated zone to reduce the residual water vapor in the IGZO.

3.5 TFT Evaluation

Mobility determines the speed of electron in channel and V_{on} indicates the power required for operation. On/off ratio ($I_{\text{on}}/I_{\text{off}}$) indicates signal contrast against noise from current leakage and is the ratio of the saturation current to the noise floor.

These parameters are extracted from the saturation current regime of the devices

using the Equation 2:

$$I_{DS}^{1/2} = \sqrt{\frac{\mu WC}{2L}} (V_{GS} - V_{on}) \quad (2)$$

where μ is the electron mobility; I_{DS} is the drain-source output saturation current; V_{GS}

is the applied gate voltage; W is the channel width length; L is channel length; and C

is the gate dielectric capacitance per unit area [20]. Sub-threshold slope (S) also

provides information of TFT device quality, related to the trap density in the interface

of semiconductor and insulator. TFT devices were tested using a Lakeshore Probe

Station (Agilent B1500). Both output curves and transfer curves were normally

collected.

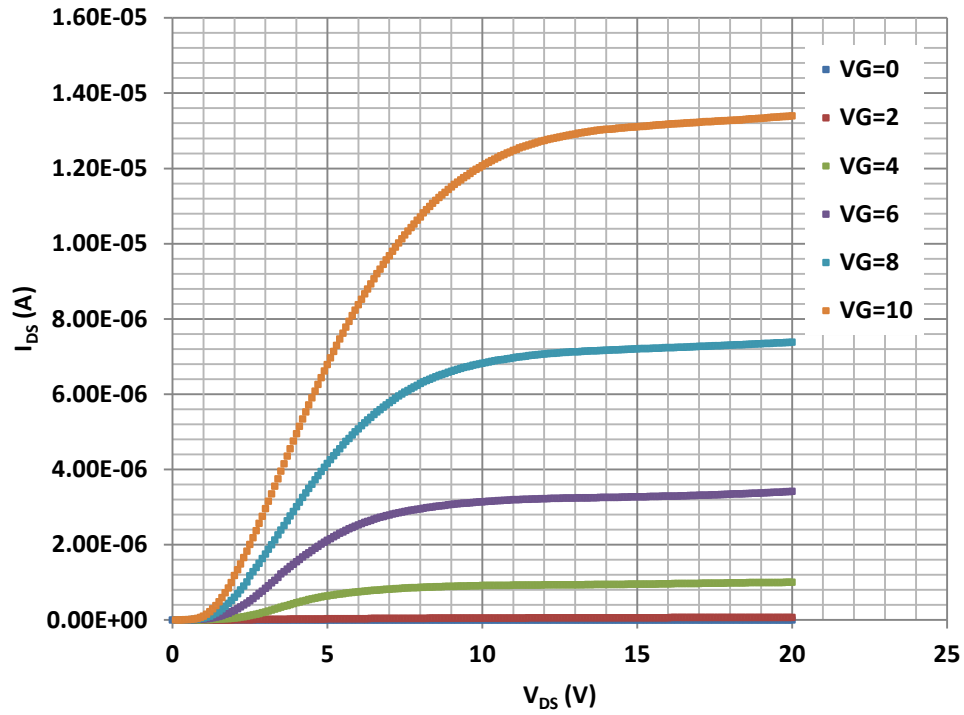


Figure 17. I_{DS} - V_{DS} curve

Figure 17 is an example of a typical output result. The source/drain voltage was swept from 0 to 20 V with gate/drain voltage at 0, 2, 4, 6, 8 and 10 V. Saturation currents were taken at V_{DS} at 20V. Figure 18 shows a plot of $(I_{DS})^{0.5}$ versus V_{DS} . The mobility is extracted from the slope $((\mu WC/2L)^{0.5})$ with the on voltage given by the intercept. The nonlinearity of $(I_{DS})^{0.5}$ - V_{DS} curve at small V_{DS} is caused by large contact resistance between IGZO and Al electrode due to post-sputter annealing in wet air.

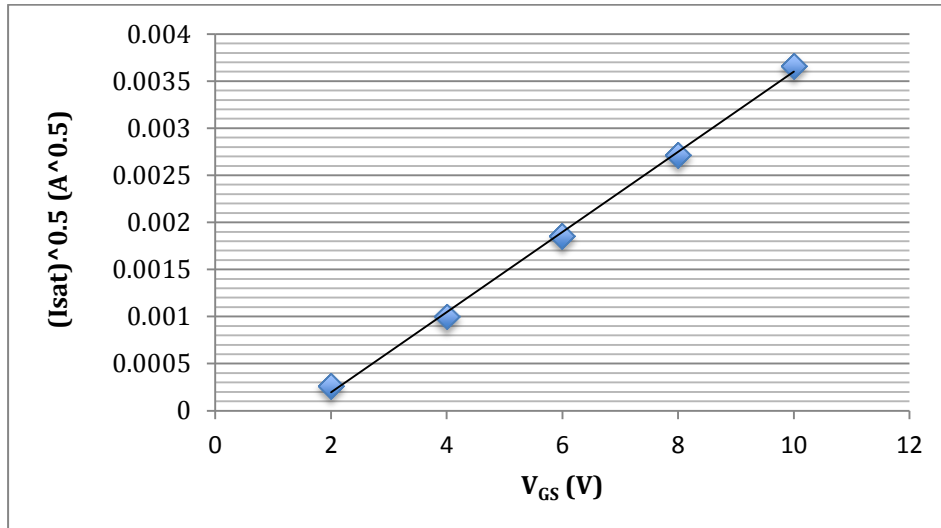


Figure 18. Fitting line of saturation current versus V_{GS} .

In addition to output curves, the transfer curve characteristics were measured as shown in Figure 19. The On/off ratio (I_{on}/I_{off}) is defined as the ratio of current at $V_{GS}=20V$ to the minimum current observed. This value is typically reported on a \log_{10} scale, $10^{6.5}$ for figure 19. The sub-threshold slope is defined as $S = dV_{GS}/d(\log_{10} I_{DS})$. As S value is dependent on V_{GS} , usually the smallest value of S is reported.

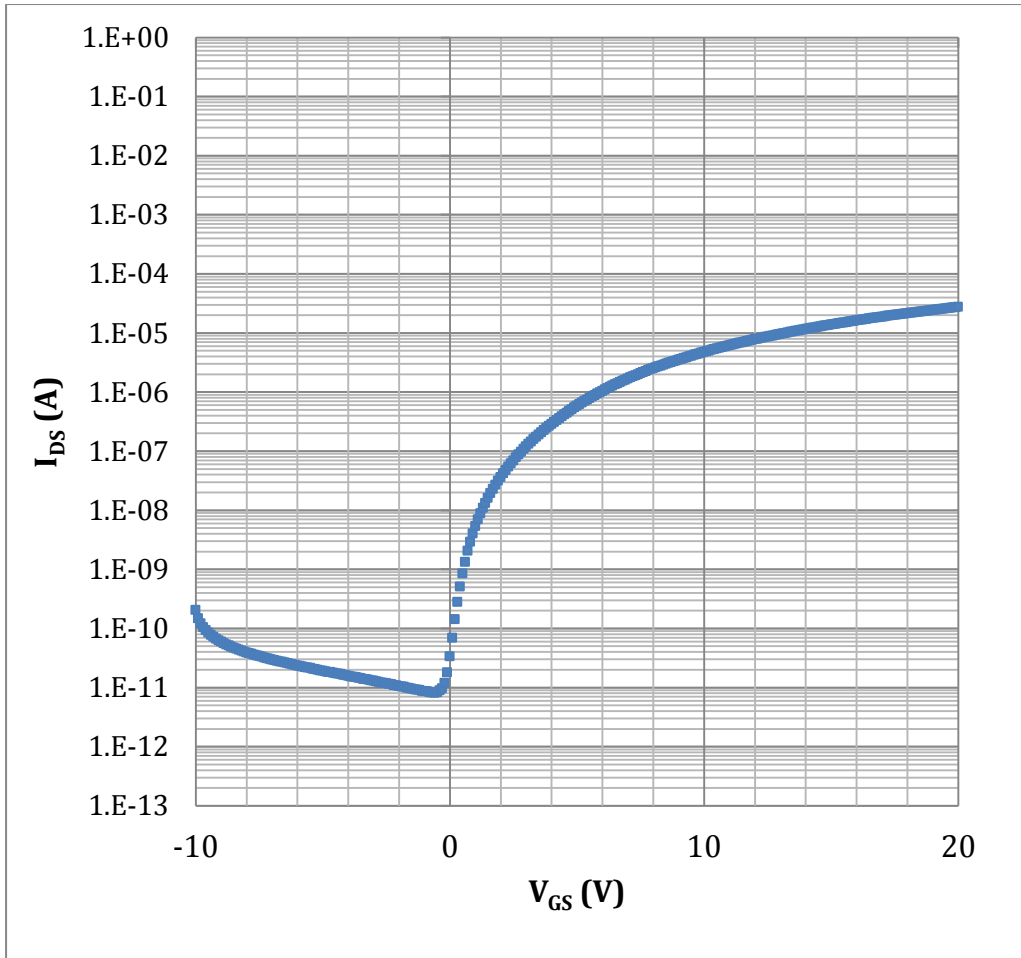


Figure 19. I_{DS} - V_{GS} curve at $V_{DS}= 10V$

Typically three devices fabricated under the same conditions were measured to obtain statistically significant results.

4. Results and Discussion

4.1 Deposition Conditions

Generally there are four parameters can be that adjusted during sputtering: pressure, power, substrate temperature and reactive composition. In this work, all depositions were done at room temperature as the IGZO film was subsequently annealed. Similarly, the gas composition was held constant with pure Ar to study properties in the non-reactive sputtering regime. Figure 20 shows the deposition rate at different operating pressure and power.

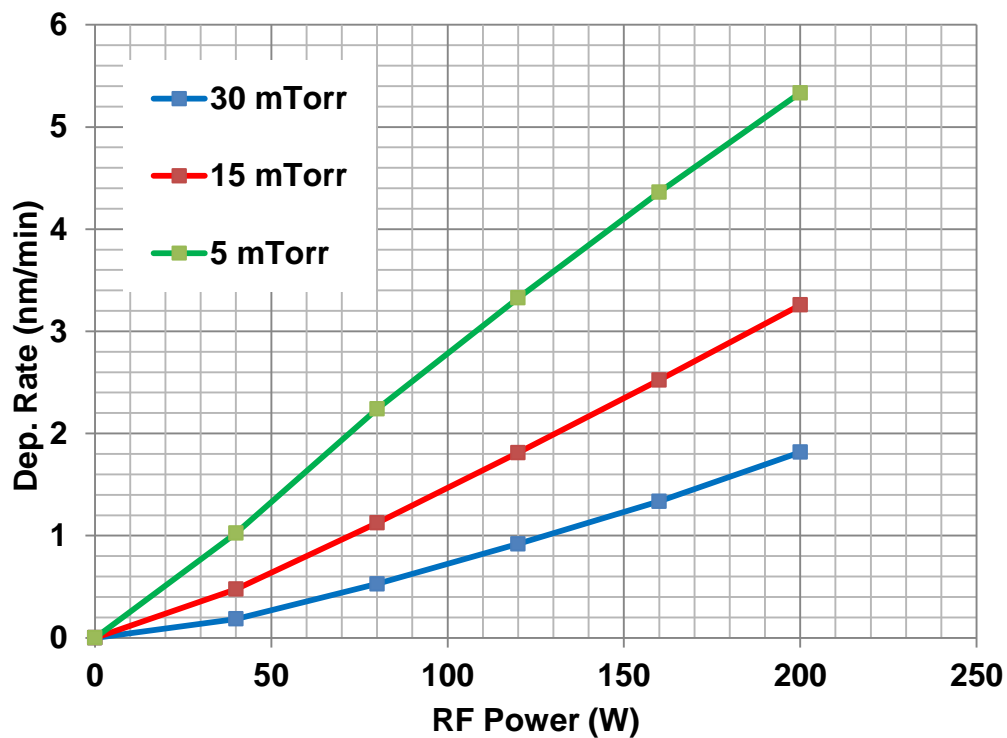


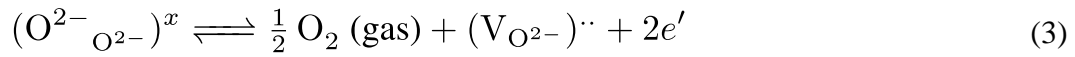
Figure 20. Sputter deposition rate at different powers and pressures

The deposition rate increases, as expected, almost linearly with RF power. Similarly, the rate increases with decreasing pressure, reaching a maximum at 5 mTorr. At 30 mTorr, the plasma is unstable because the mean free path between Ar ions is too short to accelerate and strike the IGZO target. Below 40 W, there is insufficient energy to maintain the Ar plasma in the chamber. Films deposited at 120 and 160W at 5 mTorr appeared the most uniform by eye. For these reason, 120 W and 5 mTorr was chosen as the optimized IGZO film sputtering parameters.

4.2 Reactive v.s. Non-reactive Sputtering

Reactive and non-reactive sputtering refer to characteristics of the gas ratio in the sputter chamber. In reactive sputtering, IGZO is deposited with an Ar and O₂ plasma which leads generally to stoichiometric films with low oxygen vacancy concentrations and insulator characteristics. On the other hand, IGZO film deposited by pure Ar plasma (non-reactive sputter) are initially conductive because of a high concentration of oxygen vacancies that act as donors. As Ar is significantly heavier

than oxygen, non-reactive sputtering has a higher deposition rate. The oxygen vacancy formation in these oxides is governed by equation 3



where $\text{O}^{2-}_{\text{O}^{2-}}$ indicates an oxygen atom occupying an oxygen lattice site; $\text{V}_{\text{O}^{2-}}$ is an oxygen vacancy and e' is a free (mobile) electron. The density of electrons increases as oxygen escapes from the matrix leaving oxygen vacancies. In the absence of other charged species, the carrier concentration is linearly proportion to the oxygen vacancy concentration [21].

The IGZO matrix is schematically shown in Figure 21 before and after annealing. Before annealing, non-reactive (O_2 -deficient) sputtering introduces a high oxygen vacancy concentration. The mobile electrons then give rise to an initially metallic characteristic. Furnace annealing in an oxygen environment is necessary to reduce the carrier concentration to obtain the semiconductor properties.

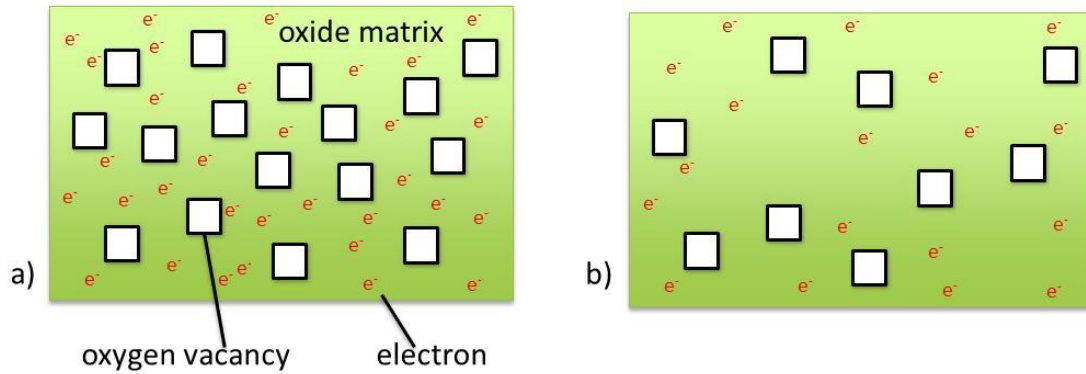


Figure 21 Schematics of IGZO a) as-deposited, showing high conductivity, and b) post-anneal in oxygen-containing ambient, showing reduced vacancy and carrier concentration.

Finding the optimized post-sputter annealing ambient is necessary for IGZO TFT fabrication.

4.3 Dry Air and Wet Air Post-sputter Annealing Ambients

Figure 22 shows the I_{DS} - V_{GS} curve of IGZO device post-annealed in dry air (dew point -62°C) and normal air with an uncontrolled $P_{\text{H}_2\text{O}}$. Surprisingly, the IGZO device post-annealed in normal air exhibited significant differences to those annealed in dry air. In particular, the V_{on} for dry air was much lower (-10V) than V_{on} for room air (-5V). As saturation current and the sub-threshold slope were similar, the primary difference is likely related to charge traps either in the IGZO or at the oxide surface. As the non-reactive sputter would have likely created films with large V_O^{2-}

concentrations, we hypothesize that P_{H_2O} is necessary to passivate or compensate these vacancies. A series of post-annealing studies were developed (Table 2) to test this hypothesis.

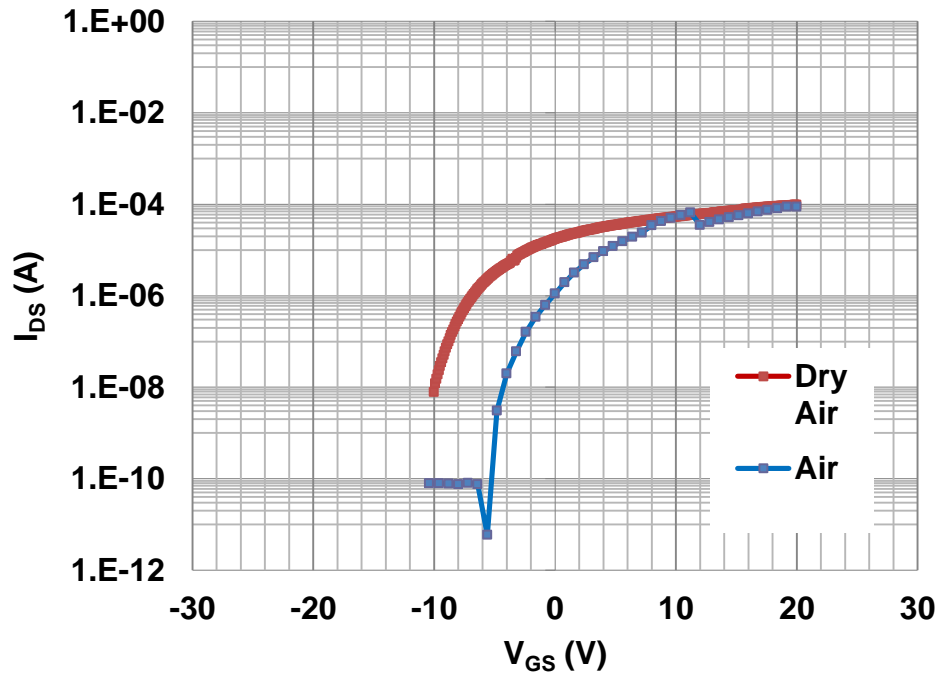


Figure 22 I_{DS} - V_{GS} curve of IGZO device post-annealed in dry air and normal air.

Table 2 Post-sputter annealing ambients studies

Dry Air ($N_2 + O_2$)
Air ($N_2 + O_2 +$ uncontrolled water vapor)
Air ($N_2 + O_2 +$ varying controlled amounts of water vapor)
N_2
N_2 + controlled water vapor
O_2
$O_2 +$ controlled water vapor

Fig. 23 shows I_{DS} - V_{GS} curves of IGZO TFTs post-sputter annealing in an ambient of dry air, and “wet” air at varying P_{H_2O} at 400°C for one hour. The wet air was saturated at 0, 10, 20 and 30°C giving p_{H_2O} =4.5, 9, 17.5 and 31.5 Torr. In all cases, the on/off ratio are on the order of $\sim 10^6$. However, with increasing P_{H_2O} , the curves shift to the right pushing V_{on} more positive. The kinks observed in curves at $V_{GS} = \sim 12$ are probably due to measurement issues.

The sub-threshold slope as a function of the P_{H_2O} is shown in Figure 24. For all conditions, the sub-threshold slope is ~ 960 mV/dec except for the highest P_{H_2O} (31.5 Torr) where it increases to 1210 mV/dec. This increase is likely due to OH^- or H^+ trapping at the interface of IGZO and SiO_2 when annealing in higher P_{H_2O} .

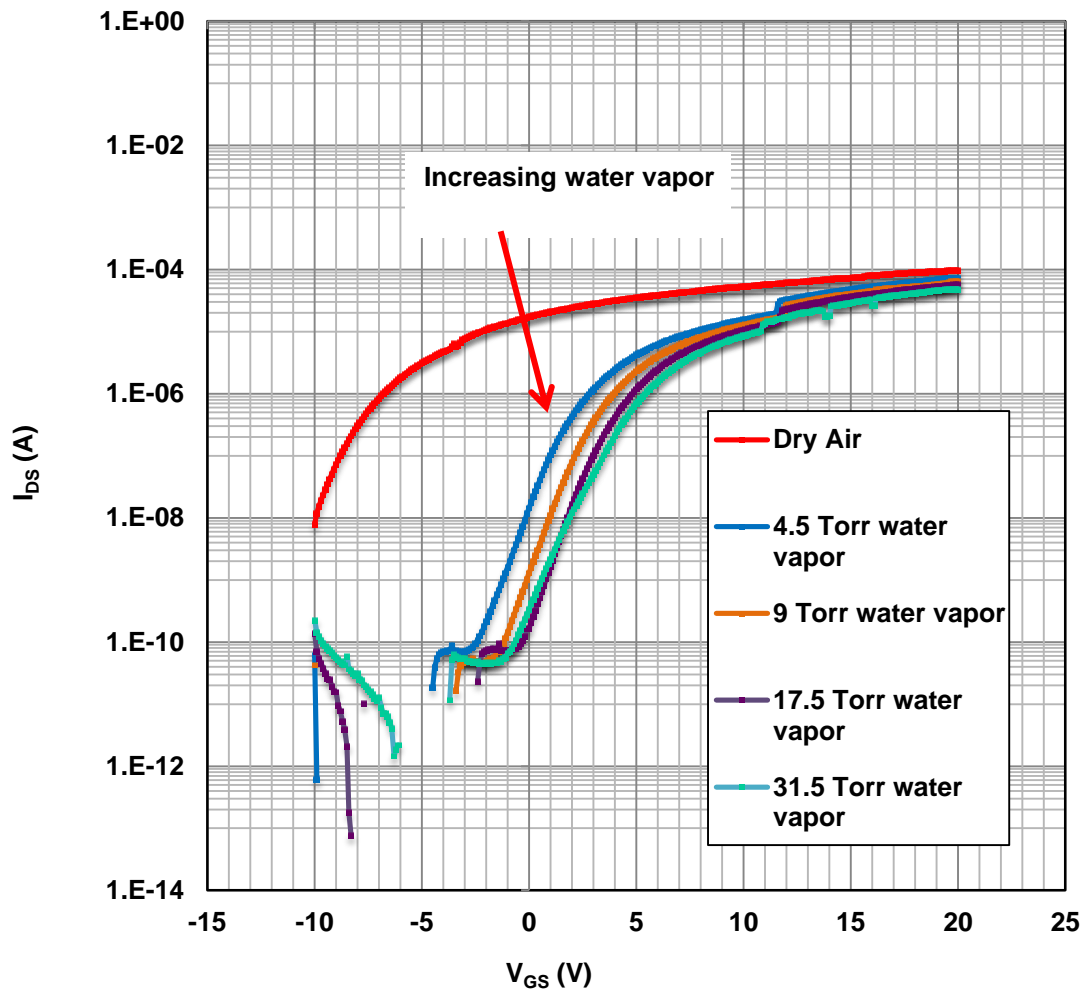


Figure 23 Transfer characteristics of IGZO devices post-annealed in air ambient with varying water vapor content. V_{DS} is 10V for all traces.

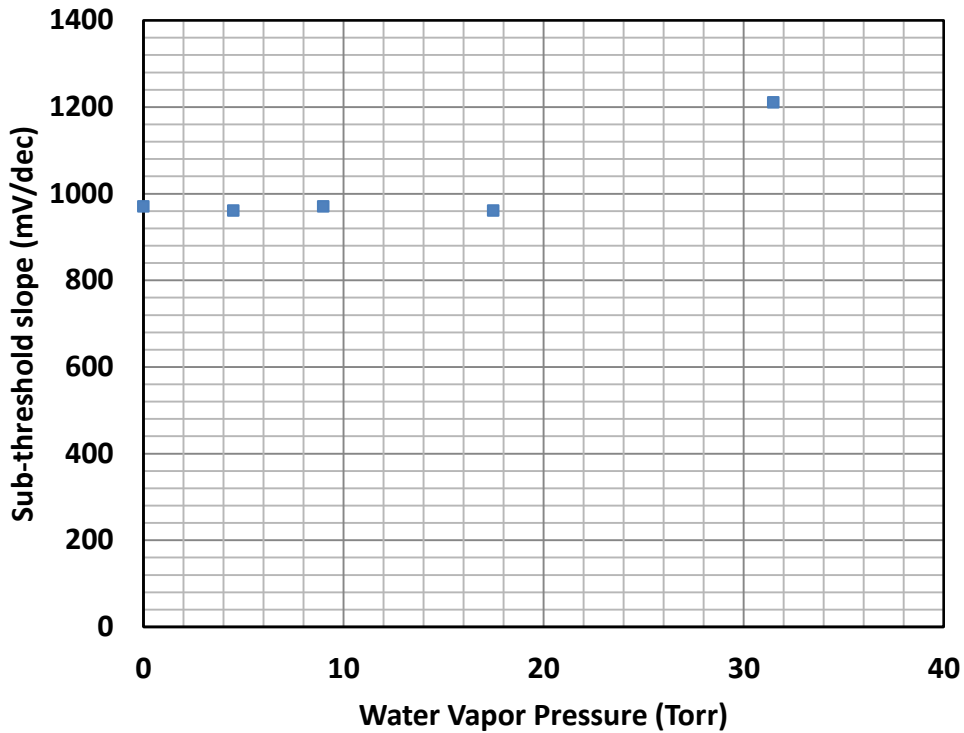


Figure 24 Sub-threshold slope of IGZO devices post-annealed in air ambient with varying water vapor content.

The mobility and V_{on} are calculated and shown in Figure 25. The V_{on} shifts dramatically with the introduction of P_{H_2O} from -8 to ~ -0.42 V. Further increases in P_{H_2O} have only a minimal change on V_{on} . The mobility however undergoes a continuous decrease from $5 \text{ cm}^2/\text{vs}$ in dry air to $\sim 2 \text{ cm}^2/\text{vs}$ at the highest P_{H_2O} level.

The on-current in the $I_{DS}-V_{GS}$ curves (Fig. 23) decreases as the water vapor increases and is consistent with the mobility decrease (Fig. 25). The addition of water vapor during annealing may impact device behavior in several ways. Upon

adsorption at the surface, H_2O can disassociate as H^+ ions, OH^- ions and O^{2-} ions.

The O^{2-} ions would be most effective in reducing the V_{O_2} - concentration and returning the IGZO to a stoichiometric composition. Both OH^- and H^+ ions can passivate charged defects, both in the bulk IGZO and at the IGZO/ SiO_2 interface. H^+ , in particular, is commonly used during amorphous semiconductor annealing to passivate dangling bonds and improve the mobility.

In the case of IGZO, the $P_{\text{H}_2\text{O}}$ does not improve the mobility; instead the mobility continuously decreases with increasing $P_{\text{H}_2\text{O}}$. Equally, $P_{\text{H}_2\text{O}}$ does not dramatically modify the interface trap density since the sub-threshold slope remains relatively unchanged for all $P_{\text{H}_2\text{O}}$'s, and increases at the highest $P_{\text{H}_2\text{O}}$. These results suggest that the dominant effect of $P_{\text{H}_2\text{O}}$ is to reduce the electron concentration through compensation of the V_{O_2} -. This shifts the device from depletion mode operation (high electron density requiring negative V_{GS} to turn off) to a conventional enhancement mode device with a positive V_{on} . Additional charge trapping at the interface may explain the reduced mobility with $P_{\text{H}_2\text{O}}$.

Oxygen is also potentially a candidate for compensation the V_{O_2} - defects.

However, dissolution of O_2 to O^{2-} is much more difficult than dissolution of H_2O .

The presence of water vapor thus appears to be critical to reduce charge types and/or vacancies present in non-reactive sputtered IGZO.

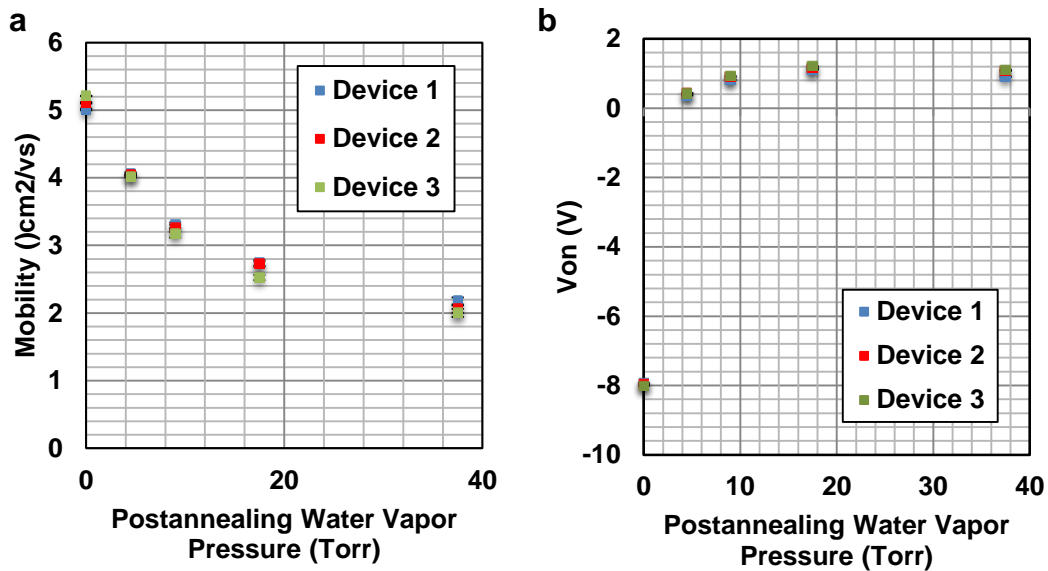


Figure 25 Mobility and on voltage of IGZO devices post-sputter annealed in air ambient with varying water vapor content.

4.4 Role of O_2 , N_2 and H_2O in post-sputter annealing

4.4.1 O_2 post-sputter annealing

Atmospheric air contains both oxygen and nitrogen (and various other gases) at a 1:4 ratio. The influence of the O_2 and N_2 were examined by annealing in ambients of pure O_2 and N_2 , as well as the pure gases with water vapor. Figure 26 compares $I_{DS}-V_{GS}$ curves of IGZO TFTs post-sputter annealed in pure O_2 and dry air. The

saturation on current after annealing in dry air is approximately twice that of samples annealing in pure O₂. However, annealing in pure O₂ shifts V_{on} toward 0 V and is similar to that observed for wet air. The enhanced P_{O₂} (5X) acts comparably to P_{H₂O} passivating V_{O₂} to reduce the electron concentration and shift V_{on} positively. However, these results also indicate that the N₂ does play a role in enhancing the mobility.

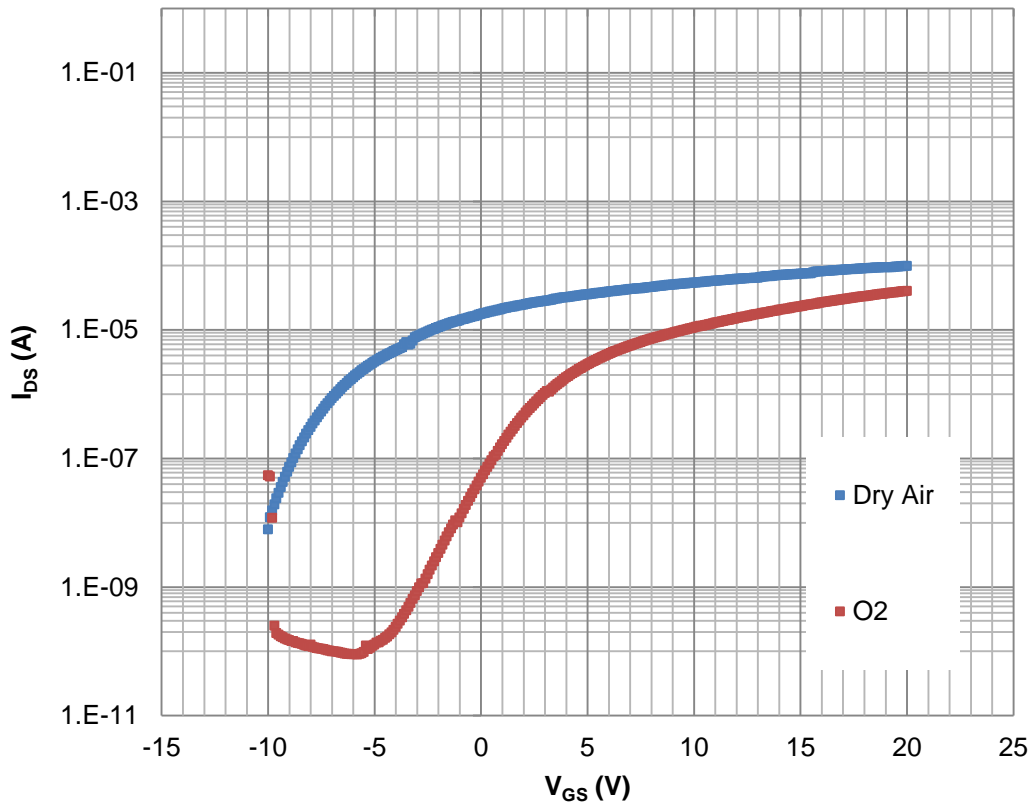


Figure 26 I_{DS}-V_{GS} curves of IGZO TFTs post-sputter annealing in ambient of pure O₂ and dry air.

4.4.2 N₂ post-sputter annealing

The role of N_2 itself in post-annealing is shown in figure 27 (a) and (b), I_{DS} - V_{GS} curves of IGZO TFTs post-sputter annealing in ambient of pure N_2 , N_2 with 9 Torr water vapor and dry air. IGZO devices post-annealed in pure N_2 exhibit high conductivity (metallic) behavior at all V_{GS} (Fig. 27 (a)). The addition of 9 Torr P_{H_2O} dramatically reduces the conductivity (factor of 5) with at least partial depletion at the most negative gate bias. However, even with P_{H_2O} , the conductivity decrease is much less than that seen in dry air annealed. It is not surprising that N_2 alone cannot compensate the oxygen vacancies in IGZO matrix. Some substitution of N on O lattice sites may be possible, but it would remain difficult to satisfy the local bonding. Water vapor does play an important role in post-annealing process, but even high P_{H_2O} would be required in the absence of O_2 .

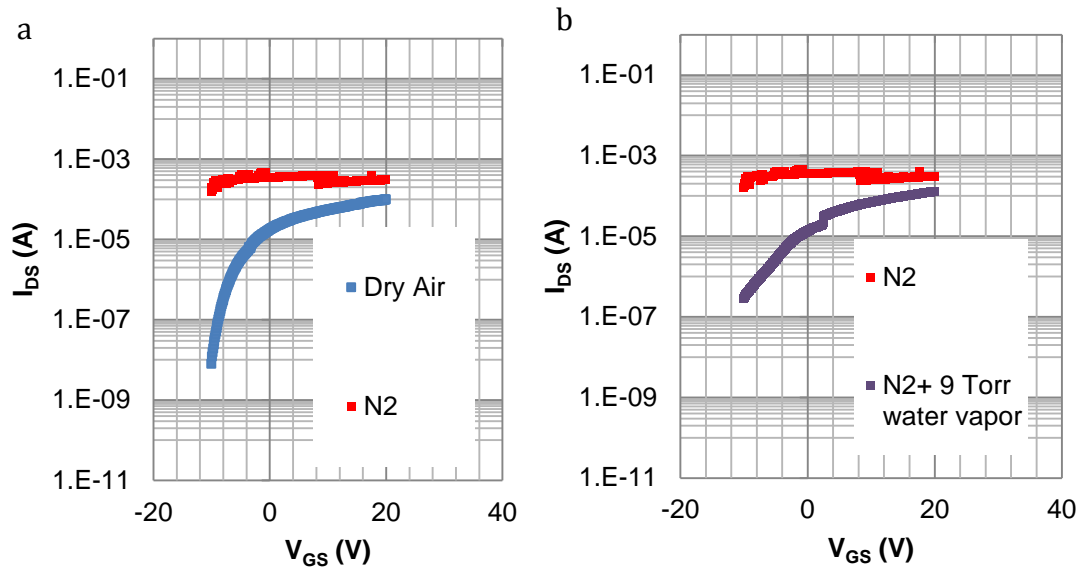


Figure 27 I_{DS} - V_{GS} curves of IGZO TFTs post-sputter annealed in pure N_2 , N_2 with 9 Torr water vapor and dry air.

4.4.3 O_2 with water vapor post-sputter annealing

The relation role of high P_{O_2} and P_{O_2} with P_{H_2O} was tested in samples annealed in pure O_2 and pure O_2 with 9 Torr P_{H_2O} (Fig. 28).

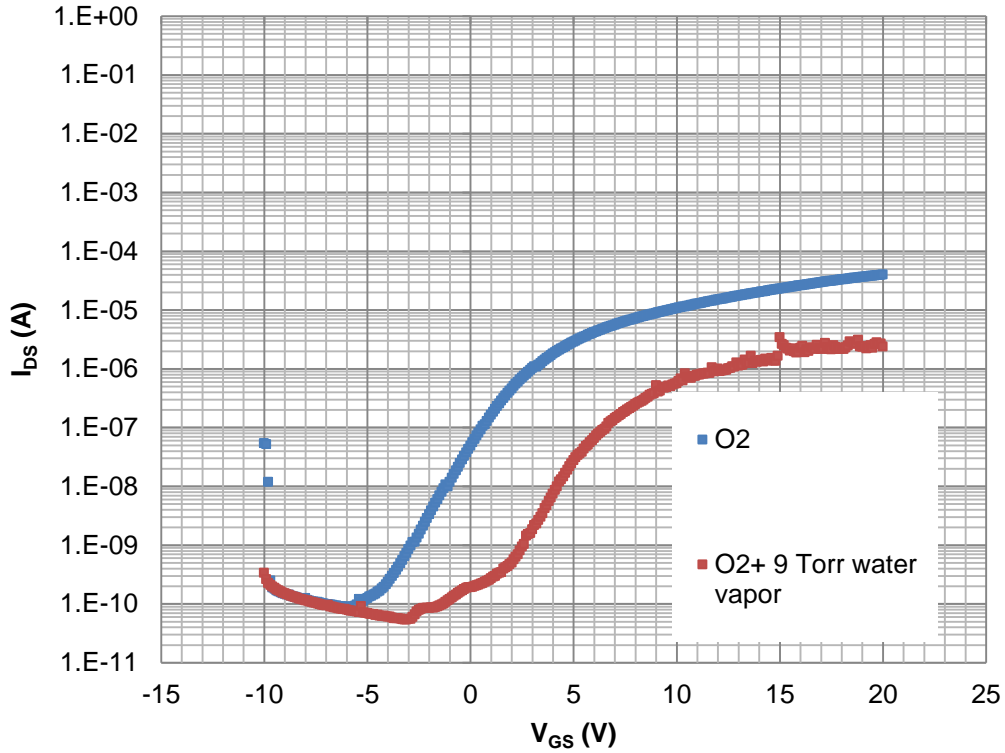


Figure 28 I_{DS} - V_{GS} curves of IGZO TFTs post-sputter annealed in pure O_2 and O_2 with 9 Torr water vapor.

The addition of P_{H_2O} to pure P_{O_2} appears to be detrimental to device properties. The on current of an I_{DS} - V_{GS} curve of O_2 with 9 Torr water vapor is reduced by one order of magnitude compared to pure O_2 , although the V_{on} has shifted more positive. This suggests that the water vapor improves the V_{on} by reducing the electron density, but it also decreases the mobility of the IGZO device.

4.4.4 O_2 with Water Vapor versus Wet Air in Post-sputter Annealing

The comparison of IGZO devices post-sputter annealed in oxygen and dry air with water vapor is shown in Figure 29. The on/off ratio of devices annealed in dry air with 4.5 Torr water vapor was 10^6 compared to $10^{5.4}$ in pure oxygen. The V_{on} in dry air with 4.5 torr water vapor was 0.42 V, while that in oxygen was 5.1 V. The improved performance with water vapor versus pure oxygen can be attributed to the smaller size of water molecules, leading to higher diffusivity in the IGZO matrix and easier compensation of oxygen vacancies.

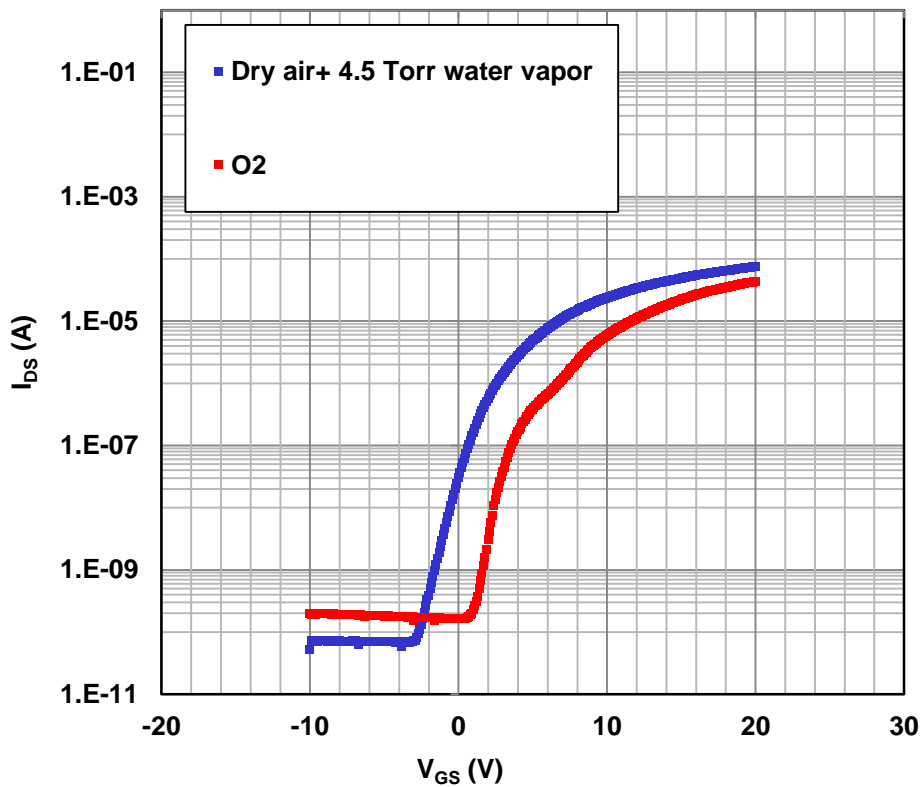


Figure 29. Comparison of transfer characteristics of IGZO devices post-annealed in oxygen and dry air with 4.5 Torr water vapor

Table 3 Performance results of all IGZO devices in different conditions

	Mobility (cm ² /vs)	V _{on} (V)
Dry Air	5.2	-8
Dry Air + 4.5 Torr water vapor	4.02	0.42
N ₂	0	X
N ₂ + 9 Torr water vapor	<<1	~0.5
O ₂	1.4	3.1
O ₂ + 9 Torr water vapor	<1	7.2

5 Summary

Table III summarize the V_{on} and mobility of devices under the varying annealing ambients. The non-reactive sputtered IGZO device post-annealed in the ambient of dry air with a small amount of water vapor (4.5 Torr) has the best performance (V_{on}) compared to dry air although it sacrifice 20% in mobility. OH^- and H^+ from water vapor act in two roles during post-annealing, one to adjust the V_{on} of IGZO device by reducing the electron concentration as vacancies are compensated, and the other one is passivation of dangling bonds. OH^- and H^+ do not induce serious interface trapping according as the sub-threshold slope remained unchanged between wet air and dry air.

6 Conclusions

The role of the annealing ambient on post non-reactive sputter deposition of IGZO has been studied. Water vapor was shown to be critical for controlling the on voltage of thin film transistor devices. The relative roles of oxygen, nitrogen and air were similarly determined. The data suggest that water vapor is critical for compensating oxygen vacancies formed by the non-reactive sputtering.

IGZO thin films were formed by non-reactive sputtering from sintered ceramic targets at room temperature. The role of the power and pressure were examined. Deposition rates increased with increasing RF power, and with decreasing pressure. Based on visual examination, optimally uniform films were obtained at a power of 120 W and an Ar pressure of 5 mTorr with deposition rates of 3.33 nm/min. These conditions were used for all subsequent studies.

As deposited IGZO films were highly conductive (metallic) corresponding to a high concentration of electrons associated with oxygen vacancies. Post-deposition annealing was critical to achieve semiconductor behavior for thin-film-transistors (TFTs). Bottom gate, bottom contact TFTs were used to evaluate the impact of the post-annealing ambient on material characteristics, particularly the mobility,

on-voltage, and the sub-threshold slope.

Annealing in "air" (at 450°C for 1 hour) resulted in devices with gate on-voltages (thresholds) near zero. However, annealing in a controlled ambient with dry air (dewpoint -62 °C) resulted in devices with a large negative turn-on voltage.

The absence of changes in the sub-threshold slope indicated that this difference was associated with the reduced compensation of as-grown oxygen vacancies in the IGZO matrix.

The behavior as a function of the water vapor pressure in controlled "dry air" was determined. With increasing $p_{\text{H}_2\text{O}}$, the turn-on voltage shifted abruptly from large negative voltages to near zero at the lowest concentrations examined ($p_{\text{H}_2\text{O}} = 4.5$ Torr). Further increases in $p_{\text{H}_2\text{O}}$ had minimal effect on the on-voltage. We believe that the water vapor is effective in compensating oxygen vacancies and hence reducing the free electron concentration in the as-deposited films. The mobility exhibited a continuous decrease with increasing $p_{\text{H}_2\text{O}}$ from $5.2 \sim \text{cm}^2/\text{V}\cdot\text{s}$ at $p_{\text{H}_2\text{O}} = 0$ Torr to $4.02 \sim \text{cm}^2/\text{V}\cdot\text{s}$ at $p_{\text{H}_2\text{O}} = 4.5$ Torr. This mobility change indicates increased charged impurity scattering at the interface from compensated defects. Except for the highest $p_{\text{H}_2\text{O}}$ conditions, the sub-threshold slope remained approximately constant

indicating no significant change in the interface trap states.

The role of p_{O_2} on annealing was examined by annealing in pure O_2 . Compared to air with $p_{O_2} = 152$ Torr, pure oxygen was more effective in compensating oxygen vacancies resulting in performance comparable to wet-air annealing. Addition of p_{H_2O} to pure O_2 did not result in any further improvements, and indeed exhibits some deleterious effects. However, results in pure O_2 were inferior to those found for annealing in wet air. This indicates that N_2 also has an effect on device annealing.

Annealing in pure N_2 , as expected, failed to compensate the oxygen vacancies and the material remained highly conductive from the as-grown oxygen vacancies.

Annealing in wet N_2 (N_2 plus p_{H_2O}) exhibited reduced conductivity, but not sufficient reduction to achieve semiconductor behavior in the TFTs. The specific role of the N_2 in the annealing has not yet been established.

The optimized condition for annealing of non-reactive sputter was determined to be dry air with 4.5 Torr of added water vapor. The 4.5 Torr p_{H_2O} is only an upper limit on the water vapor required; some p_{H_2O} is required but increasing p_{H_2O} results in lower mobility in TFT devices.

The addition of water vapor enhances the compensation of as-grown oxygen

vacancies compared to either dry air, pure oxygen, or pure nitrogen. We believe this results from the enhanced surface dissolution of H_2O to OH^- and H^+ ions, and the enhanced diffusivity of these ions compared to either molecular oxygen or atomic oxygen. Compensation of bulk oxygen vacancy defects is the dominant mechanism for improvement of device properties, though passivation of traps may also play a significant role.

7 Future works

This work has established many of the key properties but there is still much to do.

One key question is the role and need for N₂ in the annealing ambient. This should be established by adjusting the post-annealing ambients from 0% to 100% O₂ at 10% step with N₂. This will help us establish both the role of O₂ and N₂ in post-annealing process. A second key question is direct measurement of the device interface. C-V studies of the gate capacitance would directly probe trap states at the SiO₂/IGZO interface. The experiment is difficult however as IGZO has no significant acceptor states.

8 References

- [1] T. Kamiya and H. Hosono, "Material characteristics and applications of transparent amorphous oxide semiconductors," *NPG Asia Materials*, vol. 2, no. January, pp. 15–22, 2010.
- [2] K. Nomura, H. Ohta, A. Takagi, T. Kamiya, M. Hirano, and H. Hosono, "Room-temperature fabrication of transparent flexible thin-film transistors using amorphous oxide semiconductors.," *Nature*, vol. 432, no. 7016, pp. 488–92, Nov. 2004.
- [3] K. Nomura, T. Kamiya, H. Ohta, T. Uruga, M. Hirano, and H. Hosono, "Local coordination structure and electronic structure of the large electron mobility amorphous oxide semiconductor In-Ga-Zn-O: Experiment and ab initio calculations," *Physical Review B*, vol. 75, no. 3, p. 035212, Jan. 2007.
- [4] H. Yabuta, M. Sano, K. Abe, T. Aiba, T. Den, H. Kumomi, K. Nomura, T. Kamiya, and H. Hosono, "High-mobility thin-film transistor with amorphous InGaZnO₄ channel fabricated by room temperature rf-magnetron sputtering," *Applied Physics Letters*, vol. 89, no. 11, p. 112123, 2006.
- [5] H. Q. Chiang, B. R. McFarlane, D. Hong, R. E. Presley, and J. F. Wager, "Processing effects on the stability of amorphous indium gallium zinc oxide thin-film transistors," *Journal of Non-Crystalline Solids*, vol. 354, no. 19–25, pp. 2826–2830, May 2008.
- [6] H. Q. Chiang, B. R. McFarlane, D. Hong, R. E. Presley, and J. F. Wager, "Processing effects on the stability of amorphous indium gallium zinc oxide thin-film transistors," *Journal of Non-Crystalline Solids*, vol. 354, no. 19–25, pp. 2826 – 2830, 2008.
- [7] S. Hwang, J. H. Lee, C. H. Woo, J. Y. Lee, and H. K. Cho, "Effect of annealing temperature on the electrical performances of solution-processed InGaZnO thin film transistors," *Thin Solid Films*, vol. 519, no. 15, pp. 5146–5149, May 2011.

- [8] K. Ide, Y. Kikuchi, K. Nomura, M. Kimura, T. Kamiya, and H. Hosono, "Effects of excess oxygen on operation characteristics of amorphous In-Ga-Zn-O thin-film transistors," *Applied Physics Letters*, vol. 99, no. 9, p. 093507, 2011.
- [9] K. H. Ji, J.-I. Kim, H. Y. Jung, S. Y. Park, R. Choi, U. K. Kim, C. S. Hwang, D. Lee, H. Hwang, and J. K. Jeong, "Effect of high-pressure oxygen annealing on negative bias illumination stress-induced instability of InGaZnO thin film transistors," *Applied Physics Letters*, vol. 98, no. 10, p. 103509, 2011.
- [10] H. S. Shin, Y. S. Rim, Y.-G. Mo, C. G. Choi, and H. J. Kim, "Effects of high-pressure H₂O-annealing on amorphous IGZO thin-film transistors," *Physica Status Solidi (a)*, vol. 208, no. 9, pp. 2231–2234, Sep. 2011.
- [11] K. Nomura, T. Kamiya, H. Ohta, M. Hirano, and H. Hosono, "Defect passivation and homogenization of amorphous oxide thin-film transistor by wet O₂ annealing," *Applied Physics Letters*, vol. 93, no. 19, p. 192107, 2008.
- [12] J. F. Wager, "Transparent Electronics — Display Applications," *SID Symposium Digest of Technical Papers*, vol. 38, no. 1, pp. 1824–1825, 2007.
- [13] J. Plummer, *Silicon VLSI Technology Fundamental, Practice and Modeling*. New Jersey: Prentice Hall, Inc, 2000.
- [14] D. M. Mattox, *Handbook of physical vapor deposition (PVD) Processing*. New York: William Andrew Inc, 1998.
- [15] D. Smith, *Thin film deposition: principles and practice*. New York: McGraw-Hill, Inc, 1995.
- [16] P. Davidse, "Theory and practice of RF sputter," *Vacuum*, vol. 17, no. 3, 1966.
- [17] K. Wasa, M. Kitabatake, H. Adachi, *Thin film materials technology: sputtering of compound materials*. New York: William Andrew Inc, 2004.
- [18] M. Ohring, *Materials Science of Thin Films: Deposition and Structure*. San Diego: Academic Press, 2002.

- [19] R. Dammel, "Diazonaphthoquinone-based Resists," *SPIE Press*, 1993.
- [20] D. Schroder, *Semiconductor Material and Device Characterization*. New Jersey: John Wiley & Sons, Inc, 2006.
- [21] G. Wahnstrom, *Diffusion in Solid: The Minerals, Metals & Materials Society*. Pennsylvania, 1989.